Biaxial and uniaxial phases produced by partly repulsive mesogenic models involving D_{2h} molecular symmetries

Giovanni De Matteis*
Centro di Ricerca Matematica "Ennio De Giorgi," Collegio Puteano, Scuola Normale Superiore di Pisa, Piazza dei Cavalieri 3, I-56100 Pisa, Italy

Silvano Romano†
Unità di Ricerca CNISM e Dipartimento di Fisica "A. Volta," Universitá di Pavia, via A. Bassi 6, I-27100 Pavia, Italy
(Received 24 November 2007; revised manuscript received 22 April 2008; published 6 August 2008)

The present paper considers biaxial nematogenic lattice models, involving particles of D_{2h} symmetry, whose centers of mass are associated with a three-dimensional simple-cubic lattice. The pair potential is isotropic in orientation space and restricted to nearest neighbors. Let two orthonormal triads define orientations of a pair of interacting particles. The investigated potential models are quadratic with respect to the nine scalar products between the two sets of unit vectors. Actually, based on available geometric identities, these expressions can be reduced to diagonal form containing only the scalar products between corresponding unit vectors and depending on three parameters. Over the years, this comparatively simple functional form has also proven to be rather versatile. By now, various sets of potential parameters capable of producing mesogenic behavior of some kind have been proposed and studied in the literature. A new and simplified form was recently proposed and investigated by Sonnet, Virga, Durand, and De Matteis [A. M. Sonnet, E. G. Virga, and G. E. Durand, Phys. Rev. E **67**, 061701 (2003); G. De Matteis and E. G. Virga, Phys. Rev. E **71**, 061703 (2005)] and is known to support a biaxial phase at sufficiently low temperature. Following the idea of the above authors, we have studied a more extended range of parameters, including cases where biaxiality cannot be sustained in the pair ground state. In cases where a biaxial phase survives, an appropriate mean-field analysis may predict the existence of a direct second-order transition to the isotropic phase as well as a second-order sequence isotropic-to-uniaxial-to-biaxial. A second-order phase transition is also predicted, which involves isotropic and uniaxial phases only. Monte Carlo simulations have been carried out as well, for a few points in the parameter space, and found to produce results which partly confirm mean-field predictions.

DOI: 10.1103/PhysRevE.78.021702 PACS number(s): 61.30.Cz, 64.70.M−

I. INTRODUCTION

Nematogenic molecules do not possess cylindrical symmetry and sometimes have appreciable dipole moments, yet the resulting thermotropic mesophases of low-molecular weight compounds are usually uniaxial and apolar. In a number of cases, theoretical treatments have been (and still are) fruitfully simplified by assuming from the start that nematogenic molecules are $D_{\infty h}$−symmetric. On the other hand, over the last thirty years, the possible effects of molecular biaxiality (i.e., of deviations from cylindrical symmetry) on nematic order have been studied theoretically as well. By the end of the past century, molecular field (MF) [1–10] or Landau treatments [11–13], and later simulation studies of lattice models [14–18], have shown that single-component models consisting of molecules possessing D_{2h} symmetry, and interacting by appropriately chosen continuous potentials, can produce a biaxial phase. A similar scenario had emerged from the analytical study of single-component systems consisting of biaxial molecules interacting via hardcore potentials [19–27] also supported by simulation results [28–30]. In both cases, the transition between biaxial and uniaxial nematic phases is mostly found to be second order (but see below for a partly different scenario) and a direct transition between isotropic and biaxial nematic phases is predicted as well. Gay-Berne potential models (see Ref. [31] for a review), originally developed for uniaxial molecules, have been extensively investigated. More recently, biaxial extensions of them have been proposed and studied by simulation [32–38]. An extensive symmetry analysis of unconventional nematic phases was recently developed in Refs. [39–41].

Most of the above cases involve single-site models possessing D_{2h} symmetry. In a few other cases [27,30], the potential model involves two identical interacting moieties in each particle, associated with different interaction centers. Each moiety is uniaxial, and they are connected in a *V*-shaped fashion. Some other segmental or *V*-shaped models, also recently discussed in the literature, actually reduce to the single-site type [42–45]. Rigid-molecule models have been considered in the above references, and in some other cases [46–48] more general MF or simulation treatments were developed, allowing for internal (torsional) degrees of freedom.

On the experimental side, a biaxial phase had been discovered in a lyotropic system in 1980 [49]. Since 1986 there had been numerous reports of thermotropic biaxiality in low-molecular weight compounds (see, e.g., Refs. [50–53]), many of which were later called into question [54–57]. More recently [58–62], new experimental evidence of thermotropic biaxial nematic behavior has been reported in systems

*giovanni.dematteis@sns.it
†Silvano.Romano@pv.infn.it

involving polar "banana-shaped" molecules (but see also Refs. [63,64]). Evidence of this behavior has also recently been found in organosiloxane tetrapodes [65–67], as well as in polymeric systems [68,69]. The experimental search for the biaxial nematic phase is currently very active. In the last few months new findings have been published. Evidence of biaxiality has been found in the nematic phase of the boomerang-shaped mesogen ODBP-Ph-C_7 (see Ref. [70]). Moreover, the Authors of Ref. [71] reported evidence of direct first-order isotropic-to-biaxial transition in orthometallated (platinum) imine complexes. Their approach was to design metallomesogens likely to introduce lateral correlations of suitable (not too great) strength, i.e., promoting order in directions orthogonal to the main director and hence potentially stabilizing a biaxial nematic phase, but without favouring the formation of layered (smectic) ones.

Also starting a few years ago, i.e., simultaneously with and independently of the named experimental work, a renewed theoretical study of simple continuous biaxial mesogenic models was undertaken in Refs. [72–76]. The new proposed models were studied by MF, Monte Carlo simulation (MC) [77–79], and, in some cases, by two-site cluster theory [80]. Moreover, very recently and motivated by the above experimental facts, the single-tensor Landau–de Gennes theory of biaxial nematics has been carefully reexamined in Ref. [81] and a double-tensor Landau theory has been put forward and studied in Refs. [40,82].

Continuing along this line, we consider a nematogenic lattice model here, where the pair potential is restricted to nearest neighbors, and has the simplified functional form recently proposed by Durand, De Matteis, Sonnet, and Virga (DDSV) [72,73], or some extreme case thereof (see below also). The resulting behavior is investigated by MF, and comparisons are made with MC simulations, for a few points in the parameter space. More precisely, our main purpose is to single out specific cases of the general pair potential defined below, expected to produce weaker and weaker correlations between the molecular axes as the model parameters involved are varied. This approach is meant to explore to what extent the macroscopic biaxiality still survives and to determine the type of transition and the phase which forms when the biaxiality is completely suppressed.

As for the methodology employed, we recall that over the decades, mesophases possessing no positional order, such as the nematic one, have often and quite fruitfully been studied by means of lattice models involving continuous interaction potentials (see Refs. [18,44]), starting with the seminal Lebwohl-Lasher simulation paper in the early 1970's (see Ref. [83]). As noted, for example, in Ref. [44], usage of a lattice model produces significant savings in computational terms. Moreover, it entails that a number of competing phases (e.g., smectic ones), possibly preempting the nematic, are excluded from the start; notice that similar simplifications as for the possible phases are used in other named theoretical treatments as well.

Let us finally recall a few other rather recent related theoretical results: a simple MF model for biaxial smectic-A mesophases has been studied [84]. Atomistic simulations have been carried out [85] for a "banana-shaped" mesogen recently reported to produce thermotropic biaxial nematic phase [58–60]. Moreover, a biaxial mesogenic model somehow allowing for dipolar interactions has been investigated by simulation [45].

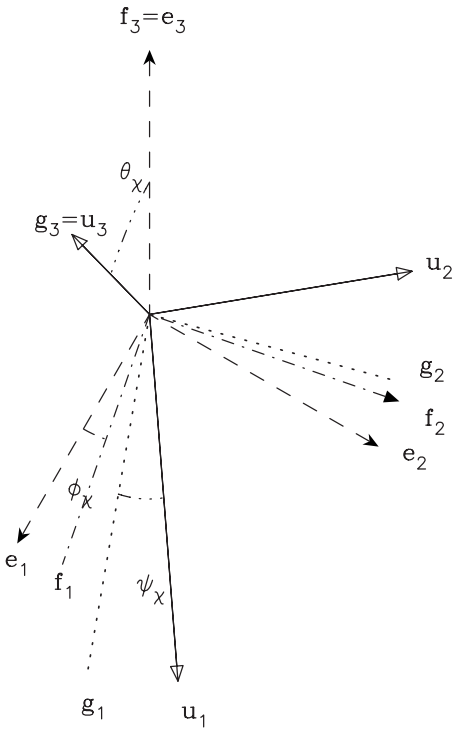

FIG. 1. Euler angles [86–88] used in the present paper. Unit vectors $\mathbf{e}_j$ denote the common laboratory frame and unit vectors $\mathbf{u}_j$ label the molecular frame, $\mathbf{f}_j$ and $\mathbf{g}_j$ correspond to the intermediate ones, introduced for the purpose of defining the angles ϕ_χ, θ_χ, ψ_χ, i.e., respectively, the azimuth, the polar angle, and the angle of proper rotation. Among these axes, $\mathbf{f}_2$ denotes the line of nodes. Laboratory axes, molecular axes, as well as the line of nodes, are marked by arrowheads.

II. GEOMETRIC IDENTITIES AND POTENTIAL MODELS

Here we consider classical identical particles possessing D_{2h} symmetry, whose centers of mass are associated with a three-dimensional (simple-cubic) lattice $\mathbb{Z}^3$. Let $\mathbf{x}_\chi \in \mathbb{Z}^3$ denote the coordinate vectors of their centers of mass.

The interaction potential will be isotropic in orientation space, and restricted to nearest neighbors, involving particles or sites labeled by χ and ρ, respectively. The orientation of each particle can be specified via an orthonormal triplet of three-component vectors (e.g., eigenvectors of its inertia tensor), say $\{\mathbf{n}_{\chi,j}, j=1,2,3\}$. In turn these are defined by an ordered triplet of Euler angles $\omega_\chi=\{\phi_\chi, \theta_\chi, \psi_\chi\}$. For the moment, let orientations be defined with respect to a common, but otherwise arbitrary, Cartesian frame $\mathbf{e}_j$ (see Fig. 1). It also proves convenient to use a simpler notation for the unit vectors defining orientations of two interacting molecules [17], i.e., $\mathbf{u}_j$ for $\mathbf{n}_{\chi,j}$ and $\mathbf{v}_k$ for $\mathbf{n}_{\rho,k}$, respectively. Here, for each j, $\mathbf{u}_j$ and $\mathbf{v}_j$ have the same functional dependences on ω_χ and ω_ρ, respectively (pairs of corresponding unit vectors in the two interacting molecules). Let $\tilde{\Omega}=\Omega_{\chi\rho}$ denote the set

of Euler angles defining the rotation transforming $\mathbf{u}_j$ into $\mathbf{v}_j$. Euler angles will be defined here according to the convention used by Brink and Satchler [86–88] (see Fig. 1). It will prove convenient for future reference to recall that, upon expressing the three unit vectors $\mathbf{n}_{\chi,j}$ in terms of Euler angles, one of them (the figure axis $\mathbf{n}_{\chi,3}$) turns out to explicitly depend on two angles ϕ_χ, θ_χ only, and a change of the third angle ψ_χ defines a rotation of the two other unit vectors around the figure axis. We also define

$$f_{jk} = (\mathbf{v}_j \cdot \mathbf{u}_k),\ G_{jk} = P_2(f_{jk}), \tag{1}$$

where $P_2(\cdots)$ denotes the second Legendre polynomial. Let us also mention for future reference that $G_{11}=1$ entails $G_{22}=G_{33}$, and similarly $G_{22}=1 \Rightarrow (G_{11}=G_{33})$, $G_{33}=1 \Rightarrow (G_{11}=G_{22})$. The nine quantities G_{jk} are not linearly independent, owing to the six constraints

$$\sum_{j=1}^{3} G_{jp} = 0, \quad \sum_{k=1}^{3} G_{qk} = 0, \quad p,q = 1,2,3. \tag{2}$$

The simplest continuous interaction potentials proposed and studied in this context (see, e.g., Refs. [4,5,72,73]) are quadratic with respect to the scalar products f_{jk}. Owing to Eqs. (2) and without any loss of generality (see, e.g., the discussion in Ref. [77]), they can be reduced to a (rather versatile) linear combination of the diagonal terms G_{kk}, i.e.,

$$\Phi = \sum_{k=1}^{3} r_k G_{kk} \tag{3}$$

or

$$\Phi = aG_{33} + b(G_{11} - G_{22}) + c[2(G_{11} + G_{22}) - G_{33}]. \tag{4}$$

Linear transformations between the two sets of coupling constants can be found in Ref. [77].

Particle interactions, correlations, and orientational order are usually expressed in terms of symmetry-adapted combinations of Wigner rotation functions $\mathcal{D}^J_{m,n}(\omega)$, i.e., for D_{2h} symmetry (see, e.g., Refs. [16,17,21])

$$R^J_{pq}(\omega) = (1/4) \sum_{s=\pm 1} \sum_{t=\pm 1} \mathcal{D}^J_{sp,tq}(\omega). \tag{5}$$

Here J, p, q denote even and non-negative integers, $0 \le p \le J$, $0 \le q \le J$, and $\omega = \{\phi, \theta, \psi\}$ denotes the ordered triplet of Euler angles. Thus

$$R^2_{00}(\omega) = P_2(\cos\,\theta),$$

$$R^2_{02}(\omega) = (1/4)\sqrt{6}\,\sin^2\theta \cos(2\psi),$$

$$R^2_{20}(\omega) = (1/4)\sqrt{6}\,\sin^2\theta \cos(2\phi),$$

$$R^2_{22}(\omega) = (1/4)(1+\cos^2\theta)[\cos(2\phi)\cos(2\psi)] - (1/2)\cos\,\theta[\sin(2\phi)\sin(2\psi)]. \tag{6}$$

Each term G_{jk} can be expressed as a linear combination of the four above functions $R^2_{pq}(\tilde{\Omega})$ (see, e.g., Refs. [21,77]). Moreover, it proves notationally convenient, especially in view of a MF treatment, to define the simpler symbols $s_k(\omega)$ as well, involving just one subscript, thus

$$s_1(\omega) = R^2_{00}(\omega), \quad s_2(\omega) = R^2_{20}(\omega),$$

$$s_3(\omega) = R^2_{02}(\omega), \quad s_4(\omega) = R^2_{22}(\omega). \tag{7}$$

On the other hand, let $\mathcal{P}$ denote a permutation of the set $\{1,2,3\}$, and let us consider the expressions

$$\Phi = ag_3 + b(g_1 - g_2) + c[+2(g_1 + g_2) - g_3],\ g_k = G_{kk}, \tag{8}$$

$$\Psi(\mathcal{P}) = \hat{a}h_3 + \hat{b}(h_1 - h_2) + \hat{c}[+2(h_1 + h_2) - h_3],\ h_k = g_{\mathcal{P}(k)}. \tag{9}$$

For a given $\mathcal{P}$, one can investigate the conditions under which $\Psi(\mathcal{P}) = \Phi$. The resulting linear and homogeneous relations connecting the two sets of coupling constants $(\hat{a},\hat{b},\hat{c})$ and (a,b,c) can be found in Ref. [77].

The above result [77] can be useful in connecting and comparing different potentials, or different notations used in the literature. The named permutations can also be used to relate potential models by duality (see, e.g., Refs. [17,72,73]). More precisely, if the above conditions are satisfied for a certain permutation $\mathcal{P}$, $|a|$ and $|\hat{a}|$ can be taken to set temperature scales, so that the two potential models [Eqs. (8) and (9)] produce the same macroscopic properties within a temperature rescaling, which can be read off the above equations. In the notation of Eq. (3), the above duality property can be given the simpler form

$$\sum_{k=1}^{3} r_{\mathcal{P}(k)} h_k = \sum_{k=1}^{3} r_k g_k \tag{10}$$

or, in other words, any relabeling of axes, coupled with the corresponding permutation of the coefficients, leaves the mutual potential energy unchanged. Notice also that the above identities are purely geometric in character, independent of the specific values of the parameters. They entail a significant reduction of the parameter space for Eq. (4) [79,89,90]. On the other hand, additional physical constraints on the parameters result, e.g., by requesting the potential to produce a biaxial ground state or/and requesting mechanical stability of it [72,73].

If at least one of the three coupling constants r_k in Eq. (3) is negative and largest in magnitude, the pair ground state can be expected to be somehow orientationally ordered (at least uniaxially ordered. The result can also be proven under more restrictive conditions). Then this "ordering" coupling constant can always be associated with the G_{33} term by a suitable relabeling of axes.

On the other hand, after stipulating that two of the three coefficients r_k in Eq. (3) be equal, a number of possible cases may be further distinguished (some of which are left for future investigation), e.g., (i) only one coefficient is simultaneously negative and largest in magnitude (the calamitic or perturbed LL scenario [72,73,77]), (ii) two of the three coefficients are negative, equal to each other, and have the largest magnitude (as in Ref. [79] and in the following μ models),

(iii) the three coefficients are negative and equal to each other [79], (iv) the three coefficients have different signs and the same magnitude, (v) the coefficient(s) with the largest magnitude is (are) positive.

Let us reconsider the notation in Eq. (4), where the coupling constants (a,b,c) have dimension of energy. It proves convenient to scale all of them by an arbitrary positive quantity ϵ with dimension of an energy and to rewrite the equation

$$\Phi = \epsilon\{a' G_{33} + b'(G_{11} - G_{22}) + c'[+2(G_{11} + G_{22}) - G_{33}]\}, \tag{11}$$

where a', b', c' are now dimensionless and ϵ is used to set energy and temperature scales (i.e., $T^* = k_B T/\epsilon$). Notice that two sets of coupling constants (a',b',c') and (a'',b'',c''), proportional by a positive quantity, can be identified, so that one can (but need not) define $\epsilon = \max\{|a|,|b|,|c|\}$, thus making the three scaled coupling constants not greater than 1 in magnitude. Thus, the rather general potential model to be investigated here reads

$$\Phi = \epsilon\{\xi G_{33} + \eta(G_{11} - G_{22}) + \zeta[2(G_{11} + G_{22}) - G_{33}]\} \tag{12}$$

or, in terms of the above symmetry-adapted basis functions [Eqs. (6) and (7)],

$$\Phi = \epsilon\left\{\xi s_1(\tilde{\Omega}) - \frac{\sqrt{6}}{2}\eta[s_2(\tilde{\Omega}) + s_3(\tilde{\Omega})] + 6\zeta s_4(\tilde{\Omega})\right\}, \tag{13}$$

where appropriate constraints on the parameters (ξ, η, ζ) producing some kind or other of nematic (especially biaxial) order are to be discussed in the following section.

At this stage it may be appropriate to comment on the different but logically equivalent notations used in the present context. On the one hand, a MF treatment ultimately reduces to a single-particle problem, where order parameters are almost directly worked out. In other words, MF essentially uses the orthogonal basis $\{s_k(\omega)\}_{k=1,\ldots,4}$ in Eq. (7). On the other hand, in simulation, the orientation of each particle is defined by three Euler angles in terms of which one constructs the three orthonormal unit vectors and hence the appropriate scalar products involving interacting pairs. Thus, the simulation essentially uses the notation in Eq. (3) for calculating potential energies and appropriate procedures for calculating order parameters as recalled in the simulation section.

When $\xi < 0$ and both $|\eta|$ and $|\zeta|$ are significantly smaller than $|\xi|$, the potential can be regarded as a perturbed Lebwohl-Lasher (LL) model, to which it reduces when $\eta = \zeta = 0$. Notice also that this choice (usually completed by setting $\xi = -1$) has been used in a number of cases. Older simulation results (to be revisited here) suggest that the condition $\xi = -1$, $\eta \neq 0$, $\zeta = 0$ entails absence of biaxial order [14].

Over the years, various specific parametrizations have been proposed and studied for Eq. (12), based on different grounds and motivations. One of them, due to Straley [4] is based on an approximate mapping from a hard-parallelepiped model. Another more often studied one is $\xi = -1$, $4\zeta = -\eta^2$. This can also be obtained by starting from a dispersion model in the London–de Boer–Heller approximation [91,92] and isotropically averaging over the orientation of the intermolecular vector (see, e.g. Refs. [5,8]). Models with fully anisotropic dispersion interactions, restricted to nearest neighbors, and associated with both two- and three-dimensional lattices, have been studied as well [42,93]. Both the Straley model [4] and the "dispersive" one mostly predict a biaxial-to-uniaxial transition of second order, followed by a uniaxial-to-isotropic transition of first order. A direct biaxial-to-isotropic transition of second order only exists for special values of the potential parameters (isolated Landau points).

An approach partly moving beyond the calamitic scenario [see previous remarks (i)–(v)] was proposed recently by DDSV. In their study, the authors [72,73] examined, for general values of the parameters, the mathematical conditions under which the pair potential (12) produces a biaxial ground state, as well as its mechanical stability. They also proposed the simplified model defined by $\xi = -1$, $\eta = 0$, $\zeta < 0$, and studied it by MF, carrying out a bifurcation analysis of the resulting consistency equations. The existence of direct transitions between biaxial and isotropic phases, was proven, together with criteria for the existence of tricritical points. More precisely, in the resulting MF phase diagram [72,73,79], the biaxial-to-uniaxial transition is found to be of second order for $0 > \zeta \gtrsim -0.20$, then of first order for $-0.20 > \zeta \gtrsim -0.22$, and finally a direct first-order transition between biaxial and isotropic phases occurs for $\zeta \lesssim -0.22$. Down to $\zeta = -(17/21) \approx -0.8095$ this transition is first order, and reverts to second order below this value. Simulation results were found to qualitatively confirm the picture [77,79]. An extensive study of the more general potential model [i.e., $\eta \neq 0$ in Eq. (12)] by bifurcation theory (as proposed in Refs. [94,21]), can be found in Ref.[89].

We are addressing here some related potential models (μ models for short) where two of the three coefficients r_j in Eq. (3) have a common value -2ϵ, and the third one is $\epsilon(1+\mu)$. We shall mostly be considering the representation $r_2 = r_3$, i.e.,

$$\Phi = \epsilon[\mu G_{11} + (-2G_{33} - 2G_{22} + G_{11})] \tag{14}$$

but let us point out that the equivalent choice $r_1 = r_2$, i.e.,

$$\Phi = \epsilon[\mu G_{33} + (-2G_{11} - 2G_{22} + G_{33})], \tag{15}$$

turns out to be more convenient in computer simulation terms. Here μ is a real positive number not greater than 1. Notice that we do not have a perturbed LL model here. Moreover, the stability analysis developed in the following section shows that a biaxial ground state survives for $\mu < 1$, and disappears when $\mu = 1$. Starting from Eq. (14) and recasting it in the form of Eq. (12), the three coefficients ξ, η, ζ can be written in terms of μ as

$$\xi = \xi(\mu) = \frac{\mu - 9}{4}, \quad \eta = \eta(\mu) = \frac{\mu + 3}{2}, \quad \zeta = \zeta(\mu) = \frac{\mu - 1}{4}. \tag{16}$$

Alternatively, upon collecting the factor $\frac{9-\mu}{4} = \max\{|\xi(\mu)|, |\eta(\mu)|, |\zeta(\mu)|\}$, one arrives at

$$\Phi = \epsilon\left(\frac{9-\mu}{4}\right)\left\{-G_{33} + 2\left(\frac{\mu+3}{9-\mu}\right)(G_{11} - G_{22}) + \left(\frac{\mu-1}{9-\mu}\right) \times [2(G_{11} + G_{22}) - G_{33}]\right\}. \tag{17}$$

The case $\mu \leq 0$ was investigated by DDSV [72–74]. On the other hand, the case $\mu = 0$ was studied in Ref. [78], and found to produce a direct biaxial-to-isotropic transition of second order. In the limiting case $\mu = +1$ (PMM model for short) the potential model becomes

$$\Phi = 2\epsilon(-G_{33} - G_{22} + G_{11}). \tag{18}$$

As for the model symbol, here potential parameters in the notation of Eq. (3) possess a common absolute value, and the capital letters correspond to their signs.

A second class of potential models to be also investigated here is defined by $\xi = -1$, $\zeta = 0$ and variable η (η models for brevity), i.e.,

$$\Phi = \epsilon[-G_{33} + \eta(G_{11} - G_{22})], \quad 0 \leq \eta \leq 1. \tag{19}$$

As the stability analysis will show, their ground state is uniaxial and not biaxial (see also the earlier remarks in Ref. [14]), also making contact with the predominant experimental situation. Moreover, in the limiting case $\eta = 1$ it becomes equivalent to the previous PMM case within numerical factors. In this case, the uniaxial ground state acquires an additional symmetry. As we shall see in the following sections, looking at the same potential model as a common limiting case of two different classes of interactions can offer some additional insight.

III. STABILITY AND INVARIANCE

It is convenient to start this section by pointing out an additional symmetry property which the general pair potential [Eq. (12)] may possess. When $\eta = 0$, two simultaneous rotations by $\pm\pi/2$ around the two unit vectors $\mathbf{u}_3$ and $\mathbf{v}_3$, respectively (i.e., taking place in the individual molecular frames), conserve the potential. In the group theoretic language this is a D_{4h} invariance of the interaction. In the parametrization of Eq. (3), this additional symmetry occurs whenever any two of the three coefficients r_j equal each other, and involves rotations around the third axes. Moreover, if one considers a sample of interacting particles on the lattice (as in the following simulations), a rotation of each of them by $\pm\pi/2$ around its third axis conserves each pair interaction and hence the overall potential energy. Thus, the named invariance property also applies to two other sets of models $3\zeta - \eta - \xi = 0$ and $3\zeta + \eta - \xi = 0$, now with respect to rotations by $\pm\frac{\pi}{2}$ around the two unit vectors $(\mathbf{u}_1, \mathbf{v}_1)$ and $(\mathbf{u}_2, \mathbf{v}_2)$, respectively. It should be noticed that the three above classes of models correspond to self-dual cases with respect to the above permutations $\mathcal{P}$ (Sec. II and Ref. [77]). Moreover, as discussed in Ref. [76], this additional symmetry may entail a reduction in the number of nonzero order parameters.

The continuous pair potential Φ in Eq. (12) or (13) admits several stationary points, where the gradient of the function vanishes. These points always include the configuration of complete alignment of corresponding unit vectors

$$\mathbf{u}_j = \pm \mathbf{v}_j, \quad j = 1,2,3. \tag{20}$$

The minimum character of the above configuration and its mechanical stability are guaranteed provided that the coupling coefficients (ξ, η, ζ) obey the following constraints [72,76]:

$$\zeta < 0 \quad \text{and} \quad |\eta| < -(\xi + \zeta). \tag{21}$$

Moreover, within the region defined by these constraints, the biaxial configuration (20) corresponds to the global minimizer of Φ. The stability region can be significantly reduced by means of the above permutations $\mathcal{P}$ to a triangular domain on the plane $\xi = -1$, bounded by the lines

$$\eta \geq 0, \quad 3\zeta - \eta + 1 \geq 0, \quad \zeta < 0 \tag{22}$$

which is the essential triangle in the terminology of Ref. [74]. This essential stability region is clearly an open set whose boundary is given by

$$\mathcal{B}_1 = \{\zeta = 0,\ 0 \leq \eta \leq 1\}, \tag{23}$$

where the local stability of the biaxial ground state breaks down. The other two sides of the triangle, that is,

$$\mathcal{B}_2 = \left\{\eta = 0,\ -\frac{1}{3} \leq \zeta < 0\right\} \quad \text{and} \quad \mathcal{B}_3 = \{3\zeta - \eta + 1 = 0,\ 0 \leq \eta < 1\}, \tag{24}$$

represent all D_{4h}-symmetric models producing stable biaxial ground state.

Since $\eta = 0$ along $\mathcal{B}_2$, then the corresponding interaction Φ turns out to be the superposition of just two, out of four, D_{2h}-symmetry-adapted functions, i.e., s_1 and s_4 [see Eq. (13)]. Actually, as also shown in Refs. [74,76], for $\eta \neq 0$, Φ can be still decomposed uniquely into two orthogonal modes as follows:

$$\Phi = -\epsilon\{a^+[v_1^+ + \sqrt{6}\gamma^+ v_2^+] + a^-[v_1^- + \sqrt{6}\gamma^- v_2^-]\}, \tag{25}$$

where $v_1^\pm = s_1 + \sqrt{6}\gamma^\pm s_3$, $v_2^\pm = s_2 + \sqrt{6}\gamma^\pm s_4$ are orthogonal D_{2h}-symmetry-adapted basis functions. Each mode corresponds to a (isotropically averaged) dispersion model at the London approximation, i.e., $\xi = -1$ and $4\zeta = -\eta^2$. Within the essential triangle (22) and on the boundary (23), provided that $\eta \neq 0$, the amplitudes (a^+, a^-) turn out to be both strictly positive in the subregion $\eta^2 < -4\zeta$ and, accordingly, the interaction is called "fully attractive". In the subregion $\eta^2 > -4\zeta$ one amplitude, that is a^+, is positive and the other, that is a^-, is negative and the corresponding pair-interaction models are called "partly repulsive".

Both classes of potential models (14) and (19) investigated here fall in the subregion of partly repulsive interac-

tions except for the extreme values $\eta=0$ and $\mu=0$, where one of the amplitudes vanishes and the interactions turn out to be attractive. The former case is the well-known LL model involving particles with $D_{\infty h}$-symmetry. The latter (Ref. [78]) is conjugated with the extremely biaxial case of the (isotropically averaged) dispersion model at the London approximation ($\xi=-1$, $4\zeta=-\eta^2$), defined in turn by $\zeta=-\frac{1}{9}$. This model also falls within the D_{4h}-symmetric potential class $3\zeta-\eta+1=0$ and yields the isolated Landau point in the phase diagram of the named dispersion model.

Let us first consider the μ models and make contact with the definitions for ξ,η,ζ we gave after Eq. (14). Since $3\zeta(\mu)-\eta(\mu)-\xi(\mu)=0$, i.e., $r_2=r_3$, then not only for $\mu=0$ but for all values of μ, the pair interaction turns out to be D_{4h} invariant. Moreover, when $\mu<1$, the above treatment proves that the potential model supports a stable biaxial ground state. Accordingly, within the essential triangle in Eq. (22), these models are entirely represented by the two sides in Eqs. (24), as also follows from the permutations $\mathcal{P}$ (Sec. II and Ref. [77]). The models defined by $\mu<0$ correspond to fully attractive interactions and they have been already investigated elsewhere [72,73,77–79]. The cases $0<\mu\leq 1$are represented by the portion $-\frac{1}{9}<\zeta\leq 0$ on $\mathcal{B}_3$.

The partly repulsive character results apparent from Eq. (14): since the coefficient μ is positive, the corresponding molecular axes repel each other with an overall magnitude $\mu+1$, while the other two terms are attractive with the same magnitude because of the D_{4h} invariance. Furthermore, from Eq. (16) one can recognize that the μ models are a superposition of an η model and an attractive term with magnitude $\frac{\mu-1}{9-\mu}$ such that the resulting potential enjoys D_{4h} invariance.

An additional, simple but telling, piece of information can be obtained: the ground-state, fully aligned configuration corresponds to a pair interaction energy $\epsilon(-3+\mu)$, whereas the two "staggered" pair configurations defined by $[G_{33}=1, G_{22}=G_{11}=-(1/2)]$ or, symmetrically, $[G_{22}=1, G_{11}=G_{33}=-(1/2)]$ correspond to an interaction energy $-\epsilon(3+\mu)/2$, and the resulting energy separation is $(3/2)\epsilon(1-\mu)$. These values suggest that, for $\mu<1$ but close to it, and at some low but finite temperatures, the "staggered" configurations may become "competitive" (both in energy and entropy terms) with the fully aligned one, and somehow disturb biaxial order.

As for a pictorial interpretation of μ models and their possible realization in practice, let us first notice that the corresponding potential can be decomposed as

$$\Phi = \mu\Phi_a + \Phi_0,$$

$$\Phi_a = \epsilon G_{11},$$

$$\begin{aligned}\Phi_0 &= \epsilon(-2G_{33}-2G_{22}+G_{11}) \\ &= \epsilon[-(G_{33}+G_{22})+(G_{32}+G_{23})],\end{aligned} \tag{26}$$

where the last expression has been obtained by using the geometric identities (2). The same identities also allow one to write the total potential in another form

$$\Phi = \epsilon[(\mu-1)(G_{33}+G_{22})+(\mu+1)(G_{32}+G_{23})]. \tag{27}$$

The term Φ_0 ($\mu=0$) can be regarded as a potential mimicking the interaction between "shape amphiphilic" mesogens containing rodlike and disclike parts covalently bonded together which have been also synthesized in the last years (see Ref. [77] and others quoted therein). The potential Φ_0 favors parallel orientation of rod moieties, parallel orientation of disc moieties, and mutual perpendicular orientations between rods and discs. Actually, $\mathbf{u}_3$ and $\mathbf{v}_3$ can be interpreted as defining (say) rod moieties, $\mathbf{u}_2$ and $\mathbf{v}_2$ can be interpreted as disc moieties, and the various terms in the pair potential Φ_0 tend to produce the above mentioned biaxial ordering effects. In addition, the geometric orthogonality constraint can also produce a recognizable amount of parallel order of the third unit vectors $\mathbf{u}_1$, $\mathbf{v}_1$, in spite of sign of the coefficient in front of it. When $\mu>0$ the contribution antinematic with respect to $\mathbf{u}_1,\mathbf{v}_1$, i.e., Φ_a, can disturb the biaxial ordering as it indirectly introduces a repulsion between the planes spanned by $\{\mathbf{u}_2,\mathbf{u}_3\}$ and $\{\mathbf{v}_2,\mathbf{v}_3\}$, respectively. This means that the tendency to biaxial order is weakened as μ is increased [see Eq. (27)]. Hence, it should be expected that in order to stabilize a homogeneous biaxial phase in the lattice, the rod-disc interaction must be suitably strong (not too large values of μ). Otherwise, the two above mentioned symmetric "staggered" configurations could prevail on biaxial ordering at finite temperature, again corresponding to the predominantly uniaxial behavior observed experimentally even for the named class of mesogens.

An alternative picture of μ models can be given by recalling that they admit the following equivalent form:

$$\Phi = \epsilon\left\{\mu P_2(\mathbf{u}_1\cdot\mathbf{v}_1) - \frac{9}{4}\sum_{s=\pm1}\sum_{t=\pm1} P_2(\mathbf{a}_s\cdot\mathbf{b}_t)\right\}, \tag{28}$$

where

$$\mathbf{a}_s = \cos(\gamma)\mathbf{u}_1 + s\sin(\gamma)\mathbf{u}_2, \quad s=\pm 1,$$

$$\mathbf{b}_t = \cos(\gamma)\mathbf{v}_1 + t\sin(\gamma)\mathbf{v}_2, \quad t=\pm 1,$$

$$2\gamma = \arccos\left(\frac{1}{3}\right) \tag{29}$$

represent the arms of two planar V-shaped (or, more precisely, and taking symmetry into account, X-shaped) interacting molecules with opening angle 2γ, where the unit vectors $\mathbf{u}_3$ and $\mathbf{v}_3$ define the directions orthogonal to the molecular planes. When $\mu=0$, the pair potential promotes biaxial ordering with $\mathbf{a}_+$ parallel to $\mathbf{b}_+$ and $\mathbf{a}_-$ parallel to $\mathbf{b}_-$, whereas if $0<\mu<1$ the biaxial alignment is disturbed by the antinematic term which can trigger, for suitably large μ, a competition of the biaxial phase with the two symmetric "staggered" configurations named above. Accordingly, an intermediate uniaxial phase could establish, characterized by uniaxial alignment of (i) $\mathbf{u}_3$ or (ii) $\mathbf{u}_2$ along a common director. In particular, the occurrence (i) could be accompanied by a totally random distribution of the molecular arms in the plane orthogonal to the main director or by a certain degree of uniaxial orientation of the molecular arms $\mathbf{a}_s$ along the

same director. The symmetric case (ii) could correspond essentially to a strong uniaxial alignment of one of the molecular arms and to a weak (or even absent) alignment of the other one around the same director.

Before considering the limiting case $\mu=1$, it is convenient to analyze the η models. These are represented by the boundary (23). As already pointed out in the previous section, $G_{33}=1 \Rightarrow (G_{11}=G_{22})$. Thus, when $0<\eta<1$, the energy of the one-parameter family of pair configurations defined by $G_{33}=1$ remains unchanged for any rotation of either interacting particles around the common direction $\mathbf{u}_3$. This degeneracy entails that the ground state cannot be biaxial. The stability analysis further shows that it is uniaxially stable [76]. This amounts to saying that the named configurations are stable under any small relative rotation tending to misalign the corresponding axes $\mathbf{u}_3$ and $\mathbf{v}_3$ so that the alignment of these two molecular axes is restored. Moreover, the one-parameter family of configurations corresponds to globally minimizing orientations for η models in Eq. (19), thus representing the ground state. In other terms, η models mimic the experimentally predominant situation where molecular interactions tend to parallelize "long axes," but produce no appreciable correlations orthogonal to it and hence orthogonal to the director.

Finally, for the PMM model ($\mu=1$ or, equivalently, $\eta=1$), in addition to the pair configurations $G_{33}=1$, the pair configurations defined by $G_{22}=1$ are similarly degenerate with respect to any rotation of the interacting molecules around the common direction $\mathbf{u}_2$. Both uniaxial (pair and, hence, ground-state) configurations are uniaxially stable, and the ground state now possesses an additional discrete symmetry. The completely aligned biaxial configuration [Eq. (20)] corresponds to the intersection of the two possible uniaxial ground states, and remains unstable. PMM is a simultaneous limiting case of both μ and η models and its ground-state degeneracies are, so to speak, inherited from both of them. Correspondingly, the above described physical interpretations are to provide a common and consistent picture. In the next sections we shall explore both classes of pair potentials, including their common limiting case, by MF and, in some cases, MC simulation.

IV. MEAN FIELD ASPECTS

The macroscopic phases which our lattice model can predict are classically labeled by four second-rank order parameters $\langle R_{pq}^2 \rangle$, ensemble averages of the above symmetry-adapted basis functions [Eqs. (5)–(7)] [95–97]. Here we use the notation $\{s_k(\omega)\}_{k=1,\ldots,4}$ introduced in Eq. (7) and the ensemble average will be computed within the MF approximation. The four named order parameters are connected with the three second–rank ordering tensors defined by

$$\mathbf{Q}_j = \left\langle \mathbf{u}_j \otimes \mathbf{u}_j - \frac{1}{3}\mathbf{I} \right\rangle, \quad j=1,2,3. \tag{30}$$

All these tensors are symmetric and traceless by construction and, moreover, they are not independent owing to the identity

$$\sum_{j=1}^{3} \mathbf{Q}_j = \mathbf{0}. \tag{31}$$

In the absence of external fields, they share one and the same eigenframe, say $\{\mathbf{e}_x,\mathbf{e}_y,\mathbf{e}_z\}$. Therefore, only four scalar parameters suffice to determine their eigenvalues. In MC simulation studies this frame is not known *a priori* and can fluctuate during simulation; instead in MF it is assumed to be known and fixed. In both treatments the orientational order is referred to this frame for allowing comparisons. Since only two out of three tensors are independent, one can form the three following pairs

$$(\mathbf{Q}_1,\mathbf{B}_1=\mathbf{Q}_3-\mathbf{Q}_2), \quad (\mathbf{Q}_2,\mathbf{B}_2=\mathbf{Q}_1-\mathbf{Q}_3),$$

$$(\mathbf{Q}_3,\mathbf{B}_3=\mathbf{Q}_1-\mathbf{Q}_2). \tag{32}$$

Then, one can select one of them and express all other quantities in terms of it. Choosing, for instance, $(\mathbf{Q}_3,\mathbf{B}_3)$ as reference pair, the following linear transformations hold:

$$\mathbf{Q}_2=-\frac{1}{2}(\mathbf{B}_3+\mathbf{Q}_3), \quad \mathbf{B}_2=\frac{1}{2}(\mathbf{B}_3-3\mathbf{Q}_3),$$

$$\mathbf{Q}_1=+\frac{1}{2}(\mathbf{B}_3-\mathbf{Q}_3), \quad \mathbf{B}_1=\frac{1}{2}(\mathbf{B}_3+3\mathbf{Q}_3). \tag{33}$$

In turn, the pair $(\mathbf{Q}_3,\mathbf{B}_3)$ can be expressed in terms of the four scalar order parameters $\{\langle s_k \rangle\}_{k=1,\ldots,4}$ as follows:

$$\mathbf{Q}_3 = S_1\left(\mathbf{e}_z\otimes\mathbf{e}_z-\frac{1}{3}\mathbf{I}\right)+S_2(\mathbf{e}_x\otimes\mathbf{e}_x-\mathbf{e}_y\otimes\mathbf{e}_y), \tag{34}$$

$$\mathbf{B}_3 = S_3\left(\mathbf{e}_z\otimes\mathbf{e}_z-\frac{1}{3}\mathbf{I}\right)+S_4(\mathbf{e}_x\otimes\mathbf{e}_x-\mathbf{e}_y\otimes\mathbf{e}_y), \tag{35}$$

where $S_1=\langle s_1\rangle, S_2=\sqrt{\frac{2}{3}}\langle s_2\rangle, S_3=\sqrt{6}\langle s_3\rangle, S_4=2\langle s_4\rangle$, obey the following constraints (see also Ref. [76]):

$$-\frac{1}{2}\le S_1\le 1, \quad -\frac{1}{3}(1-S_1)\le S_2\le\frac{1}{3}(1-S_1),$$

$$-(1-S_1)\le S_3\le(1-S_1), \tag{36a}$$

$$-\frac{1}{3}\min\{2+S_1+3S_2+S_3,2+S_1-3S_2+S_3\}\le S_4$$

$$\le\frac{1}{3}\min\{2+S_1-3S_2+S_3,2+S_1+3S_2-S_3\}. \tag{36b}$$

From the above tensorial representation, it is apparent that $\langle s_1\rangle$ and $\langle s_2\rangle$ represent uniaxial and biaxial ordering of the molecular axis $\mathbf{u}_3$, respectively. The ordering of the other two molecular axes $\mathbf{u}_1$ and $\mathbf{u}_2$ is globally represented by $\langle s_3\rangle$ and $\langle s_4\rangle$: the former characterizes the uniaxial one and the latter the biaxial one. Similarly, the transformed tensors $(\mathbf{Q}_1,\mathbf{B}_1)$ and $(\mathbf{Q}_2,\mathbf{B}_2)$ admit a representation similar to $(\mathbf{Q}_3,\mathbf{B}_3)$ with the corresponding four scalar components yielded by the linear relations (33). Thus, the two transformed components

pertaining to $\mathbf{Q}_1$ ($\mathbf{Q}_2$) describe the uniaxial and biaxial ordering of $\mathbf{u}_1$ ($\mathbf{u}_2$), while the ones pertaining to $\mathbf{B}_1(\mathbf{B}_2)$ describe the global ordering of the other two molecular axes $\mathbf{u}_2,\mathbf{u}_3$ ($\mathbf{u}_1,\mathbf{u}_3$).

Physically speaking, the three pairs of tensors provide a different measure of orientational order. Actually, the single tensor $\mathbf{Q}_j$ provides a direct measure of the degree of alignment of the single molecular axis $\mathbf{u}_j$, and the difference between the three degrees of alignment is particularly relevant in connection with a pair potential model Φ involving different signs and different magnitudes of the coefficients r_1,r_2,r_3 in Eq. (3) [see remarks (i) to (v) in Sec. II], and thus both attractive and repulsive couplings. A natural procedure for assigning the order parameters at a given temperature, consists of finding first the largest eigenvalue of each of the tensors $\mathbf{Q}_j$. Then the largest eigenvalue among the ones determined in the first step is selected. The value so obtained, say $\bar{\lambda}$, provides the actual new $\langle s_1\rangle$ order parameter via $\langle s_1\rangle = \frac{3}{2}\bar{\lambda}$. The first procedure is equivalent to a set of symmetry transformations to be applied to the order parameters and it corresponds to permutations of the eigenvectors $\{\mathbf{e}_x,\mathbf{e}_y,\mathbf{e}_z\}$ of both $\mathbf{Q}_j,\mathbf{B}_j$ simultaneously and for each j [76,79]. As a consequence of these transformations the four order parameters of each pair $(\mathbf{Q}_j,\mathbf{B}_j)$ can be appropriately recast to provide a positive and maximum value of $\langle s_1\rangle$. The second procedure results in a further discrimination among the eigenvalues of the three pairs $(\mathbf{Q}_j,\mathbf{B}_j)$ which aims at selecting the pair where $\mathbf{Q}_j$ conveys the most calamitic molecular axis, that is the largest value of $\langle s_1\rangle$. The overall methodology mimics the one usually employed in MC simulations for detecting uniaxial and biaxial phases [16,28,96]. In this section we discuss the results obtained when the above approach is applied, within a MF treatment, to both μ and η models.

After applying a MF procedure (see also references quoted in the introduction) and starting from the order parameters defined in Eqs. (34) and (35), the resulting expression for the free energy in the general case in Eq. (12) reads

$$A^*_{\mathrm{MF}} = 3\sum_{j=1}^{4}\sum_{k=1}^{4} d_{jk}\langle s_j\rangle\langle s_k\rangle - T^*\ln[\Xi/(8\pi^2)],$$

$$\Xi = \int_{\mathrm{Eul}} \exp(\beta\tilde{W})d\omega, \tag{37}$$

$$\tilde{W} = 6\sum_{j=1}^{4}\sum_{k=1}^{4} d_{jk}\langle s_j\rangle s_k(\omega), \quad \beta = 1/T^*. \tag{38}$$

Here $\int_{\mathrm{Eul}}$ denotes integration over Euler angles, i.e., for any integrable function $\mathcal{F}(\omega)$

$$\int_{\mathrm{Eul}} \mathcal{F}(\omega)d\omega \equiv \int_0^{2\pi} d\phi \int_0^{\pi} \sin\theta d\theta \int_0^{2\pi} \mathcal{F}(\omega)d\psi, \tag{39}$$

and asterisks mean scaling by ϵ. The symmetric matrix D with entries d_{jk} is defined by

$$[D] = \begin{bmatrix} -\xi & 0 & +\frac{\sqrt{6}}{2}\eta & 0 \\ 0 & -2\xi & 0 & +\sqrt{6}\eta \\ +\frac{\sqrt{6}}{2}\eta & 0 & -6\zeta & 0 \\ 0 & +\sqrt{6}\eta & 0 & -12\zeta \end{bmatrix} \tag{40}$$

and its four eigenvalues $\{\nu_j\}$ can be written in a compact way:

$$\nu_3 = 2\nu_1,$$

$$\nu_4 = 2\nu_2,$$

$$\nu_{1,2} = (1/2)(\mathcal{R} \mp \sqrt{\mathcal{S}}), \tag{41}$$

where

$$\mathcal{R} = -\xi - 6\zeta,$$

$$\mathcal{S} = (\xi - 6\zeta)^2 + 6\eta^2. \tag{42}$$

Within the domain of biaxial ground-state stability, represented by the constraints in Eq. (22), it turns out that $\nu_2 > 0$, whereas $\nu_1 \geq 0$ provided that $\eta^2 \leq -4\zeta$. Accordingly, the fully attractive or partly repulsive character of the underlying microscopic interaction is reflected by the spectrum of D and the dispersion parametrization produces two zero eigenvalues. Moreover

$$\frac{\partial A^*_{\mathrm{MF}}}{\partial\langle s_j\rangle} = 6\sum_{k=1}^{4} d_{jk}\tau_k, \quad j = 1,2,3,4, \tag{43}$$

$$\tau_k = \langle s_k\rangle - (1/\Xi)\int_{\mathrm{Eul}} s_k(\omega)\exp(\beta\tilde{W})d\omega, \quad k = 1,2,3,4, \tag{44}$$

so that the four consistency conditions $\tau_k = 0$ entail the extremum equations

$$\frac{\partial A^*_{\mathrm{MF}}}{\partial\langle s_j\rangle} = 0, \quad j = 1,2,3,4. \tag{45}$$

The consistency equations are satisfied at all temperatures by the set $\langle s_k\rangle = 0$, entailing $A^*_{\mathrm{MF}} = 0$ (the isotropic solution). At sufficiently low temperature, other values of $\langle s_k\rangle$ define acceptable solutions, producing $A^*_{\mathrm{MF}} \leq 0$.

Since the potential models under investigation [Eqs. (14), (18), and (19)], represent partly repulsive pair interactions, the corresponding MF free-energy A^*_{MF} fails to possess a global minimum in the order parameter space in correspondence of the solutions of the consistency equations. The search for the stable phases has then to be conducted through a minimax principle, proposed and justified in Ref. [74] within the MF approximation for biaxial nematics and originally put forward by Bogolubov, Jr. in other contexts [98–100]. In order to apply a minimax procedure we let E define the 4×4 Hessian matrix whose entries E_{ij} consist of the second

derivatives of A^*_{MF} with respect to four parameters $\{\langle s_k\rangle\}_{k=1,\ldots,4}$, calculated in the found solution(s) of the consistency equations. In practice, the minimax procedure requires first solving the consistency equations, usually, by a bifurcation technique [101,102]. Next, at each examined temperature, and for each found solution, one has to consider the above Hessian matrix E, and check its eigenvalues: locally stable solutions are those where the above matrix possesses at most two negative eigenvalues and these are candidates to stable phase(s). Eventually, among them, the one with the lowest free energy is selected so that a locally stable solution may define the stable one over some temperature range. Thus, when applied globally, the minimax procedure yields, at a given temperature, the minimal value of A^*_{MF} over the discrete set of solutions of the consistency equations. The order parameters of the stable phases so obtained are then to be recast according to the double-step recipe outlined above in order to be compared with MC results.

As for the μ models [Eq. (14)] the corresponding D matrix is obtained by setting $\xi=\xi(\mu)$, $\eta=\eta(\mu)$, $\zeta=\zeta(\mu)$ and letting μ range in $]0,1]$. As shown in the previous section, these models turn out to be D_{4h} symmetric. The corresponding symmetry transformation ($\pm\frac{\pi}{2}$ rotation around $\mathbf{u}_1$ and $\mathbf{v}_1$) entails the following identity between the order tensors

$$\mathbf{Q}_2=\mathbf{Q}_3, \quad \mathbf{B}_2=\mathbf{B}_3, \tag{46}$$

meaning that the recipe illustrated above needs to be applied only to $(\mathbf{Q}_1,\mathbf{B}_1)$ and $(\mathbf{Q}_3,\mathbf{B}_3)$. By the MF treatment worked out in Refs. [74,76], the additional D_{4h} invariance may also entail that just two out of the four actual order parameters suffice for the description of a condensed phase. Actually, it is possible to show that the above D_{4h} symmetry can result in some constraints on the order parameters, i.e.,

$$\langle s_3\rangle=\langle s_2\rangle \tag{47a}$$

$$\langle s_1\rangle=2\langle s_4\rangle+\sqrt{\frac{8}{3}}\langle s_2\rangle, \tag{47b}$$

thus giving rise to a reduction of the free order parameters. When applied *a priori*, this constrained analysis is equivalent to a restricted MF (RMF) approximation. Solutions obeying Eqs. (47) can correspond to biaxial phases involving all four order parameters with $\langle s_2\rangle$ and $\langle s_3\rangle$ vanishing as $T^*\to 0$ and $\langle s_1\rangle\to 1$, $\langle s_4\rangle\to\frac{1}{2}$ in the same limit [see bounds (36)].

A detailed unconstrained numerical bifurcation analysis has been carried out here. From now on we shall be using the terms restricted (or constrained) MF and unconstrained MF, or simply MF.

Let us start from the isotropic state. According to the minimax stability criterion, this state is a locally stable solution, and actually the stable phase, provided that

$$T^*>\Theta_{\mathrm{MF}}=\frac{18}{5} \quad \forall\,\mu\in[0,1]. \tag{48}$$

At $T^*=\Theta_{\mathrm{MF}}$ the isotropic state becomes unstable and a new solution of the consistency equations bifurcates. Thus, an ordered phase condenses in the lattice leading to a second-order phase transition. The (unconstrained) MF treatment has shown that when $\mu<\mu_1\approx 0.43$, the order parameter profiles of the established phase comply with Eqs. (47) and, accordingly, the model supports a direct isotropic-to-biaxial phase transition (see Figs. 2–5). When $\mu_1<\mu<1$, an intermediate uniaxial stable phase bifurcates at $T^*=\Theta_{\mathrm{MF}}$ from the isotropic phase, and minimizes the unconstrained free-energy in the range of temperatures $\Theta_{\mathrm{MF}}>T^*>T_A(\mu)$, where $T_A(\mu)$ decreases to zero as μ tends to 1. On the other hand, at the temperature Θ_{MF} the above reduced solution [Eqs. (47)] keeps bifurcating and turns out to be the global minimizer only for $T^*<T_B(\mu)<T_A(\mu)$, where $T_B(\mu)$ also decreases to zero as μ goes to 1. In the interval $[T_B,T_A]$, whose amplitude tends to zero as μ approaches to 1, a biaxial phase involving all four order parameters is established, which differs from

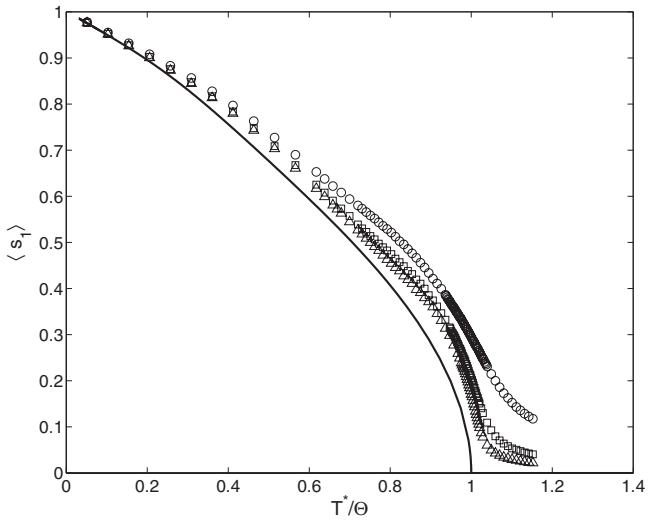

FIG. 2. MF predictions (continuous curve) and simulation results (discrete symbols) for the order parameter $\langle s_1\rangle$ of the μ model defined by $\mu=\frac{1}{4}$, obtained with different sample sizes. Circles: $l=10$, squares: $l=20$, triangles: $l=30$. As pointed out in the text, here and in the following figures, Θ denotes the respective transition temperature, i.e., Θ_{MF} for the MF and Θ_{MC} for the MC results.

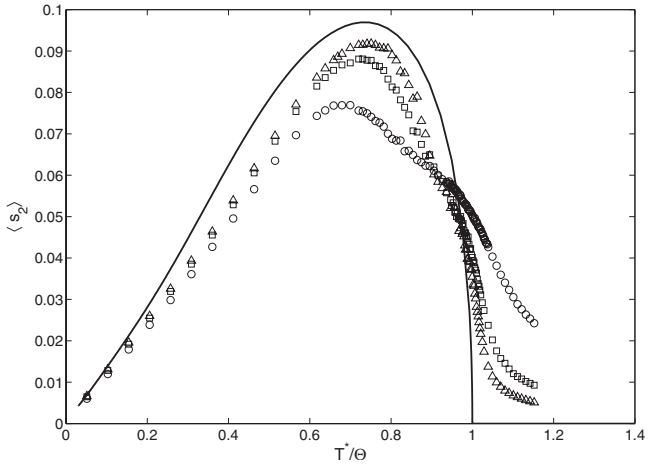

FIG. 3. MF predictions (continuous curve) and simulation results (discrete symbols) for the order parameter $\langle s_2\rangle$ of the μ model defined by $\mu=\frac{1}{4}$, obtained with different sample sizes. Same meaning of symbols as in Fig. 2.

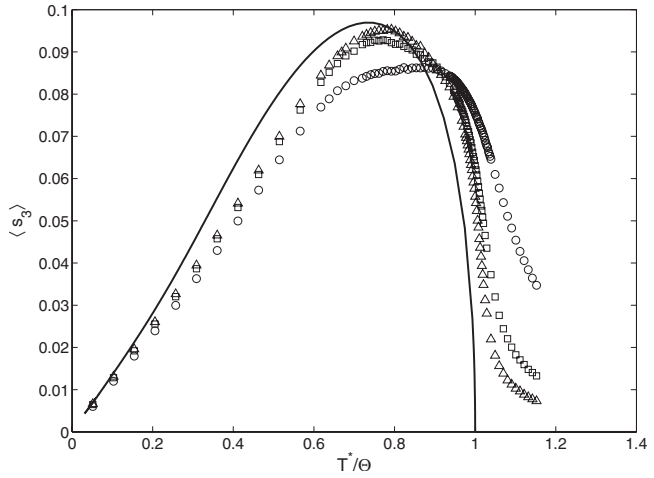

FIG. 4. MF predictions (continuous curve) and simulation results (discrete symbols) for the order parameter $\langle s_3 \rangle$ of the μ model defined by $\mu=\frac{1}{4}$, obtained with different sample sizes. Same meaning of symbols as in Fig. 2.

the one in Eqs. (47) and continuously connects the minimizers for $T^* \geq T_A$ to those ones for $T^* \leq T_B$, thus bridging the gap. In Figs. 6–9 the order parameters for $\mu=\frac{3}{4}$ are represented by heavy solid curves and compared with MC simulation results (see also the following section). The points $\{\mathsf{A}_k, \mathsf{B}_k\}_{k=1,\ldots,4}$ in the plots mark the order parameters $\{\langle s_k \rangle\}_{k=1,\ldots,4}$ at the temperatures T_A, T_B. It should be noticed that the order parameters $\langle s_1 \rangle$, $\langle s_2 \rangle$, and $\langle s_3 \rangle$ exhibit a nonmonotonic dependence on T^*: more precisely, $\langle s_1 \rangle$ increases as temperature is decreased up to a relative maximum at $T^*=T_A$, where it abruptly starts decreasing and then, at $T^*=T_B$, it increases again up to the saturation value 1. As for the remaining order parameters, $\langle s_2 \rangle$ and $\langle s_4 \rangle$ are predicted to be zero (within numerical accuracy) in the range $T^* \geq T_A$, then $\langle s_2 \rangle$ increases rapidly, attains a maximum value at $T^*=T_B$ and tends to zero as $T^* \to 0$. $\langle s_4 \rangle$ keeps increasing start-

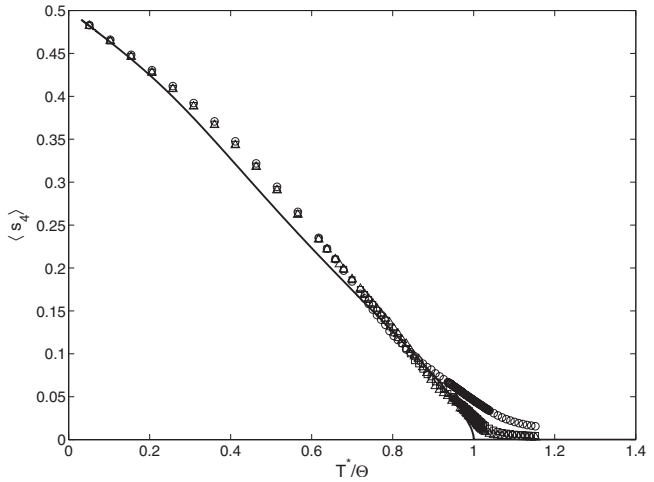

FIG. 5. MF predictions (continuous curve) and simulation results (discrete symbols) for the order parameter $\langle s_4 \rangle$ of the μ model defined by $\mu=\frac{1}{4}$, obtained with different sample sizes. Same meaning of symbols as in Fig. 2.

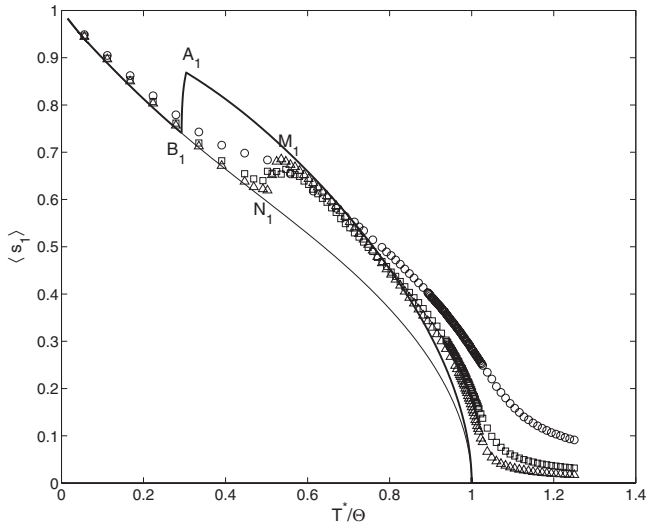

FIG. 6. MF predictions and simulation results for the order parameter $\langle s_1 \rangle$ of the μ model defined by $\mu=\frac{3}{4}$. The heavy solid continuous curve marks results obtained by means of an unconstrained MF approximation, involving four order parameters. The light solid line marks the MF results obtained when the reduction of order parameters is applied (RMF treatment, see also text). The points A_1 and B_1 mark the order parameters at $T_A(\frac{3}{4})$ and $T_B(\frac{3}{4})$, respectively, where the unconstrained analysis predicts additional transitions with abrupt changes of slope. For $T^* < T_B$, heavy and light curve overlap. Discrete symbols represent simulation results for the same model, obtained with different sample sizes. Same meaning of symbols as in Fig. 2. Points M_1 and N_1 mark MC results discussed in the text.

ing from zero at $T^*=T_A$ and up to its maximum value $\frac{1}{2}$. The order parameter $\langle s_3 \rangle$ starts increasing at the takeover of the ordered phase, i.e., $T^*=\Theta_{\mathrm{MF}}$, then it approaches a local maximum and at $T^*=T_A$, when already decreasing, it starts increasing again up to a second local maximum at $T^*=T_B$ and, eventually, decreases to zero as $T^* \to 0$. In the same figures the reduced order parameters [Eqs. (47)] are plotted as light solid curves which turn out to be superimposed to the heavy ones for $T^* < T_B$. To summarize, the (unconstrained) MF analysis predicts first a uniaxial-to-biaxial transition, and then another transition involving biaxial phases; they are continuous and marked by abrupt changes of slope at T_A and T_B, respectively. Thus, our analysis, and comparisons with MC results to be mentioned later, show that the above reduction holds over some range of μ values, that is at all temperatures when $\mu < \mu_1$, and for the biaxial phase stable at the lowest temperatures, that is, $T^* < T_B(\mu)$, when $\mu > \mu_1$.

The above profile structure is typical in the range $\mu_1 < \mu < 1$ and yields the global MF phase diagram plotted in Fig. 10 together with MC estimates of transition temperatures for a few selected μ values; numerical values of the transition temperatures are collected and compared in Table I as well; comparison between MF and MC predictions for the order parameters will take place in the following. At this stage, on the basis of MF results only, we could attempt a physical interpretation of the above temperature dependence of the order parameters. As remarked in the previous section, the model parameter μ is a measure of the strength of repul-

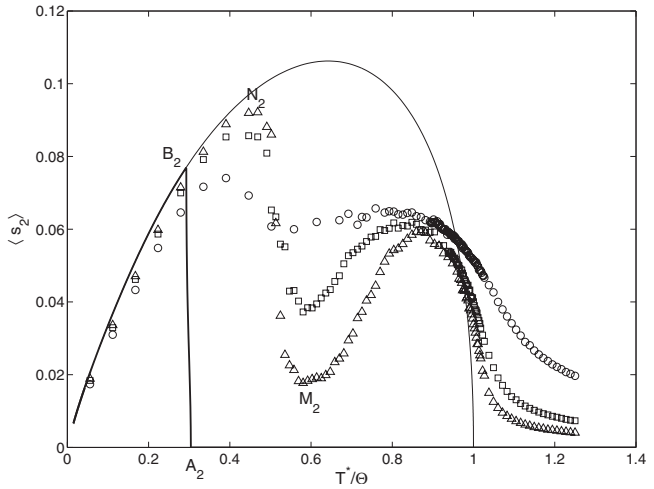

FIG. 7. MF predictions and simulation results for the order parameter $\langle s_2 \rangle$ of the μ model defined by $\mu=(3/4)$. As in Fig. 6, the heavy solid continuous curve marks the result obtained by means of an unconstrained MF treatment, involving four order parameters. The light solid line marks the MF result when the reduction of order parameters is applied (RMF treatment, see also text). The points A_2 and B_2 mark the order parameters at $T_A(\frac{3}{4})$ and $T_B(\frac{3}{4})$, respectively, where additional transitions take place with abrupt changes of slope. For $T^* < T_B$ heavy and light curves overlap. The unconstrained MF treatment predicts $\langle s_2 \rangle = \langle s_4 \rangle = 0$ for $T^* > T_A$, i.e., a uniaxial phase (see also Fig. 9). Discrete symbols represent simulation results for the same model, obtained with different sample sizes. Same meaning of symbols as in Fig. 2. The points M_2 and N_2 mark MC results discussed in the text.

sion between two corresponding molecular axes [see Eq. (14)]. Notice that, according to the order parameter reconstruction presented above, the choice of the pair of mutually repelling molecular axes [Eq. (14) or (15)] does not affect the resulting order parameter profiles. As far as μ is not too big ($\mu < \mu_1$), the repulsion is not sufficient to prevent the biaxial phase from forming directly from the isotropic phase:

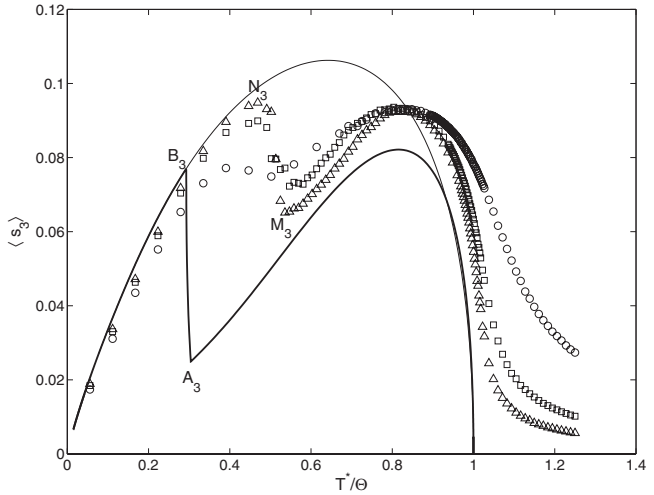

FIG. 8. MF predictions and simulation results for the order parameter $\langle s_3 \rangle$ of the μ model defined by $\mu=(3/4)$. The meaning of symbols corresponds to the two previous Figs. 6 and 7.

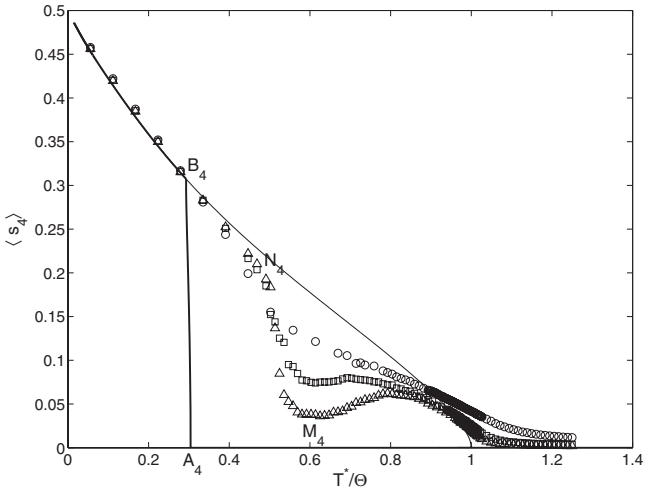

FIG. 9. MF predictions and simulation results for the order parameter $\langle s_4 \rangle$ of the μ model defined by $\mu=(3/4)$. The meaning of symbols corresponds to the three previous Figs. 6–8. Notice also that the unconstrained MF treatment predicts $\langle s_2 \rangle = \langle s_4 \rangle = 0$ for $T^* > T_A$, i.e., a uniaxial phase (see also Fig. 7).

all three molecular axes are sufficiently correlated and aligned to let the biaxial phase condense in the lattice. As μ is increased ($1 > \mu > \mu_1$), the stronger repulsion brings disorder in the lattice at high temperatures and, by cooling

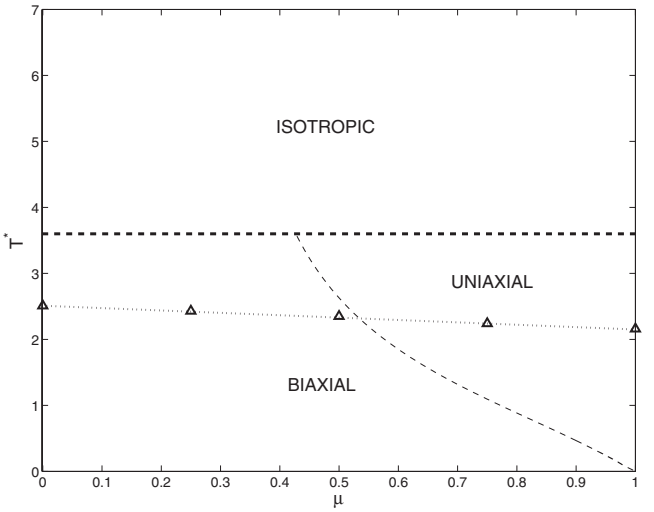

FIG. 10. MF phase diagram for the μ potential models [Eq. (14)]. The ordering transitions are second order, and the lowest-temperature phase involved is predicted to be biaxial for $0 \leq \mu < 1$, and uniaxial when $\mu=1$ (PMM model; see also text). Discrete symbols (triangles) represent MC simulation results for transition temperatures, and the straight dotted line was obtained by least-square fit. The light dashed line marks the temperature $T_A(\mu)$ joining the line $T^* = \Theta_{\mathrm{MF}} = \frac{18}{5}$ at $\mu = \mu_1 \approx 0.43$. According to the MF predictions, in the range $T_A(\mu) < T^* < \Theta_{\mathrm{MF}}$ an intermediate uniaxial phase takes place and the uniaxial-to-biaxial transition is second order. The corresponding MC simulation results obtained with $\mu=3/4$ suggest a weakened biaxial phase (see also text). The curve $T_B(\mu)$, marking biaxial-to-biaxial transitions (see also text), nearly coincides with $T_A(\mu)$ to the resolution of the figure. Numerical results are collected in Table I.

TABLE I. MF and MC estimates for transition temperatures, obtained for potential models defined by different values of μ in Eq. (14).

μ	Θ_{MF}	Θ_{MC}	T_A	T_B
0[78]	18/5	2.51 ± 0.01		
1/4	18/5	2.43 ± 0.01		
1/2	18/5	2.35 ± 0.01	2.6285	2.6279
3/4	18/5	2.24 ± 0.01	1.0948	1.0543
1 (PMM)	18/5	2.15 ± 0.01		

down from the isotropic phase, the first phase which forms is a uniaxial one, where both order parameters $\langle s_1 \rangle$ and $\langle s_3 \rangle$ are nonzero. By a further decrease in temperature, a transition to the biaxial régime is expected to take place at $T^*=T_A$, and the phase is correctly described by the above RMF solution at even lower temperatures $T^*<T_B$. The transition shows a recognizable decrease of $\langle s_1 \rangle$, which can be seen as reflecting the above competition mechanism [see Sec. III before Eq. (27)]; moreover, by the relevant definitions [Eqs. (6) and (7)], a decrease of $\langle s_1 \rangle$ tends to produce an increase of $\langle s_3 \rangle$ via its θ-depending term; in other words, if the cone described by a molecular axis, say $\mathbf{u}_3$, around $\mathbf{e}_z$ widens, the alignment of the other two (described by $\langle s_3 \rangle$) around the same director $\mathbf{e}_z$ increases. Actually, the order parameter $\langle s_3 \rangle$ may also increase owing to the biaxial environment.

Before discussing the results obtained at $\mu=1$, it is convenient to illustrate the predictions for the second class of potential models under investigation [Eq. (19)]. For these latter models the D matrix is specialized by setting $\xi=-1$, $\zeta=0$, and letting η range in $[0,1[$. For $\eta=0$, the well-known Maier-Saupe or LL model is recovered in our setting. The model supports a first-order transition between isotropic and uniaxial nematic phase taking place at $\Theta_{\mathrm{MF}} \simeq 1.3212$; this model was also extensively studied by a number of other techniques, including simulation [18,103–107], whose estimate for the transition temperature is $\Theta_{\mathrm{MC}} = 1.1232 \pm 0.0001$. When $\eta>0$, the partly repulsive nature of the interaction [see Sec. III after Eq. (25)] requires us to enforce a minimax strategy. For this class of interaction models, there are no internal symmetries leading to an *a priori* reduction of the order parameter space. Therefore the bifurcation analysis has to be performed in the whole space of order parameters. On the other hand, as shown in the previous section, the ground state suggests the absence of biaxial order at all temperatures and the following analysis will confirm the expectation, thus showing *a posteriori* that one can legitimately work out a mean-field treatment based on the uniaxial order parameters only.

Let us now summarize the results of the above MF analysis in terms of its locally stable solutions. Their number is always 2 for $0 \leq \eta \leq 1$. For $0 \leq \eta \leq 1$ the isotropic phase is locally stable at temperatures above its supercooling limit $T_c^*(\eta)$, defined by

$$T^* > T_c^* = T_c^*(\eta) = \frac{3 + 9\eta^2 + 3\sqrt{1+3\eta^2}}{5\sqrt{1+3\eta^2}}, \tag{49}$$

notice that $T_c^*(\eta=0)=\frac{6}{5}$, as already known for the Maier-Saupe model. As for the orientationally ordered phase, numerical bifurcation analysis shows that for $0<\eta \leq 1$ the only locally stable solutions of the four consistency equations, entail $\langle s_2 \rangle = 0 = \langle s_4 \rangle$ and the only nonvanishing order parameters are the uniaxial ones, i.e., $\langle s_1 \rangle$ and $\langle s_3 \rangle$, as previously disclosed on the basis of ground-state considerations. The consistency equations for the uniaxial phase reduce to

$$\langle s_1 \rangle = \frac{\int_0^\pi \exp[3\beta(2\langle s_1 \rangle + \sqrt{6}\langle s_3 \rangle \eta) s_1(\vartheta)] I_0\left(\frac{9}{2}\langle s_1 \rangle \beta \eta \sin^2\vartheta\right) s_1(\vartheta) \sin\vartheta d\vartheta}{\int_0^\pi \exp[3\beta(2\langle s_1 \rangle + \sqrt{6}\langle s_3 \rangle \eta) s_1(\vartheta)] I_0\left(\frac{9}{2}\langle s_1 \rangle \beta \eta \sin^2\vartheta\right) \sin\vartheta d\vartheta}, \tag{50}$$

$$\langle s_3 \rangle = \frac{\sqrt{6}\int_0^\pi \exp[3\beta(2\langle s_1 \rangle + \sqrt{6}\langle s_3 \rangle \eta) s_1(\vartheta)] I_1\left(\frac{9}{2}\langle s_1 \rangle \beta \eta \sin^2\vartheta\right) \sin^3\vartheta d\vartheta}{4\int_0^\pi \exp[3\beta(2\langle s_1 \rangle + \sqrt{6}\langle s_3 \rangle \eta) s_1(\vartheta)] I_0\left(\frac{9}{2}\langle s_1 \rangle \beta \eta \sin^2\vartheta\right) \sin\vartheta d\vartheta} \tag{51}$$

where I_0 and I_1 are modified Bessel functions of the first kind and indices 0 and 1, respectively. These equations correspond to the ones for a uniaxial phase consisting of D_{2h}-symmetric molecules given in Ref. [5], where the authors studied the geometric mean approximation model, i.e., $\xi=-1$, $4\zeta=-\eta^2$ in our setting.

In order to illustrate the typical scenario arising from these models, we choose $\eta=\frac{1}{4}$, also for a comparison with MC simulation studies reported in the following. For this selected value, the supercooling limit of the isotropic phase can be read from Eq. (49) as $T_c^*(\eta=\frac{1}{4}) = \frac{12\sqrt{19}+57}{20\sqrt{19}} \approx 1.2538$. For $T^* < \Theta_{\mathrm{MF}} \approx 1.3468$ the isotropic phase is accompanied

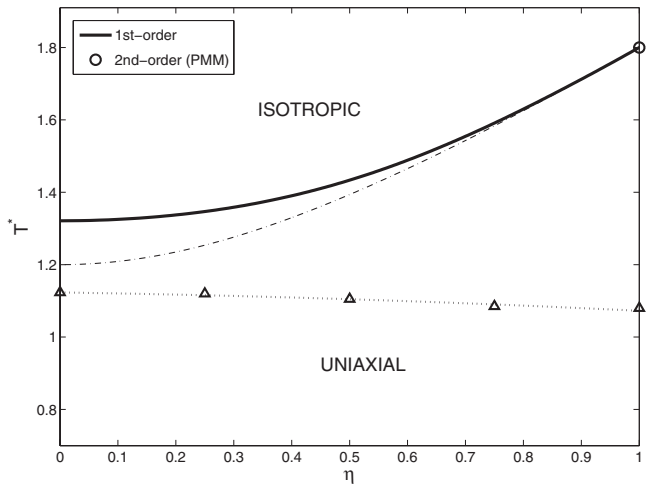

FIG. 11. MF Phase diagram for the η-potential models [Eq. (19)]. The thick solid line marks first-order transitions from isotropic to uniaxial phase. The thin dashed-dotted line represents the bifurcation points from the isotropic state [supercooling limit $T_c^*(\eta)$, see Eq. (49)]. Both lines meet at the PMM model where the transition becomes second order (isolated tricritical point, see text), and is marked by a circle. Accordingly, the precocity p (see text) tends to zero as η tends to 1. Discrete symbols (triangles) represent MC simulation results for transition temperatures. The dotted line, obtained by least-square fit, corresponds to a very flat parabola (see also text). Numerical results are collected in Table II.

by another locally stable solution, globally minimizing the free-energy A_{MF}^* according to the minimax criterion, and actually defining the stable phase. This is a positive-ordered uniaxial phase with $\langle s_1 \rangle$ saturating at the upper bound 1 and, accordingly, $\langle s_3 \rangle$ at 0 [see bounds in Eqs. (36)]. Thus, a first-order transition occurs from the isotropic phase, which establishes a uniaxial phase with both the order parameters $\langle s_1 \rangle$ and $\langle s_3 \rangle$, characterizing a general uniaxial phase produced by biaxial molecules.

Numerical continuation in η shows that the solution found for $\eta=\frac{1}{4}$ stays qualitatively unchanged for $0<\eta<1$ and yields the global phase diagram in Fig. 11. In this figure we represent the transition line (solid heavy line) that marks all first-order transitions from the isotropic to the uniaxial phase, i.e., the temperature Θ_{MF} as a function of η. The thin dashed-dotted line represents the supercooling temperature $T_c^* < \Theta_{\mathrm{MF}}$ as a function of η. This latter curve meets the transition line at $\eta=1$, meaning that there the transition changes from first to second order. Thus, MF predicts that, upon increasing η, the transition temperature increases, whereas its first-order character weakens, again in rough agreement with MC results. In Table II both MF and MC predictions for the transition temperatures are reported for a few selected values of η. Finally, for $\eta=1$, the scenario changes in two ways: on the one hand, $\Theta_{\mathrm{MF}}(\eta=1) = T_c^*(\eta=1)$, i.e., the transition between isotropic and uniaxial nematic phases turns second order. On the other hand, the above MF treatment also returns a biaxial solution, now locally unstable at all temperatures. Recall that this case can also be regarded as the limit of the μ models as $\mu \to 1$, where the two above temperatures T_A and T_B vanish. In other words, in terms of η models, the additional D_{4h} invariance at $\eta=1$, causes the order of transition to change from first to second, whereas the condensed phase remains unchanged, and its uniaxial character is a signature of the ground state. Strictly speaking, PMM represents for the η models an isolated tricritical point on the isotropic-to-uniaxial transition line. Accordingly, as η tends to 1 the quantity $p=\frac{[\Theta_{\mathrm{MF}}(\eta)-T_c^*(\eta)]}{\Theta_{\mathrm{MF}}(\eta)}$, the so-called precocity [108], goes to zero as a consequence of the molecular biaxiality.

In the next section a MC simulation study will be presented for both η and μ models, and a comparison with the above MF predictions will take place.

V. SIMULATION ASPECTS

The potential models defined by $\mu=(1/4),(1/2),(3/4)$, $\eta=(1/4),(1/2),(3/4)$, and $\eta=\mu=1$ were studied by MC simulation as well. Calculations were carried out on a periodically repeated cubic sample, consisting of $N=l^3$ particles, $l=10,20,30$, and were run in cascade, in order of increasing temperature. Each cycle (or sweep) consisted of $2N$ MC steps, including a sublattice sweep [109]. The finest temperature steps used were $\Delta T^*=0.005$, and even $\Delta T^*=0.0025$, in the transition regions (see below).

Equilibration runs took between 250 00 and 200 000 cycles, and production runs took between 250 000 and 1 250 000. Macrostep averages for evaluating statistical errors were taken over 1000 cycles. Calculated thermodynamic quantities include mean potential energy per site U^* and configurational specific heat per particle C^*, where the asterisks mean scaling by ϵ and k_B, respectively. Simulation estimates of the order parameters $\langle R_{pq}^2 \rangle$ [95–97] were calculated by

TABLE II. MF estimates for transitional properties, obtained for potential models defined by different values of η in Eq. (19), and MC estimates for the corresponding transition temperatures; at $\eta=1$ the transition becomes second order.

η	Θ_{MF}	$\langle s_1 \rangle$	$\langle s_3 \rangle$	ΔU_{MF}^*	$\langle P_4 \rangle$	Θ_{MC}
0[103–107]	1.3212	0.4292		0.5521	0.1200	1.1232 ± 0.0001
1/4	1.3468	0.3818	0.0256	0.4553	0.0955	1.120 ± 0.005
1/2	1.4335	0.2448	0.0414	0.2171	0.0405	1.105 ± 0.005
3/4	1.5912	0.0942	0.0282	0.0412	0.0064	1.085 ± 0.005
1 (PMM)	18/10					1.075 ± 0.005

analyzing a configuration every cycle, using methodologies discussed in detail by other authors [16,28,96]. We also evaluated the so-called short-range order parameters [95,96]

$$\sigma_{L,j} = \langle P_L(\mathbf{u}_j \cdot \mathbf{v}_j) \rangle, \quad L = 2,4, \quad j = 1,2,3, \tag{52}$$

measuring correlations between corresponding pairs of unit vectors associated with nearest-neighbor molecules. It follows from Eq. (12) that the potential energy U^* is a linear combination of the quantities $\sigma_{2,j}$. Moreover, for μ models, the D_{4h} symmetry of Eq. (14) entails $\sigma_{L,3} = \sigma_{L,2}$. Actually, simulation results obtained for $\mu < 1$ were found to produce results satisfying this condition within associated statistical errors; on the other hand, preliminary simulations carried out for $\mu = 1$ yielded $\sigma_{L,3} \neq \sigma_{L,2}$, in the orientationally ordered region at low temperatures. This we interpreted as a reflection of the above ground-state degeneracy, as well as of the fact that, at low temperatures, interconversion between the two ground-state configurations (or, in general, between ordered configurations rather close to them) has to overcome a significant energy barrier, and becomes too slow with respect to the named MC procedure. Therefore, in the case $\mu = 1$, at the end of each macrostep, we carried out a rotation of each particle by $\pi/2$ around its $\mathbf{u}_1$ axis. Simulation results obtained in this way for $\sigma_{L,j}$ were found to satisfy the above symmetry condition within associated statistical errors.

This collective rotation can (but need not) be used for $\mu < 1$ as well: additional tests showed that, in these cases, calculations carried out both with and without implementing the named procedure yielded consistent results for the observables of interest, i.e., in agreement within associated statistical uncertainties. Simulations of the μ models were actually performed using the equivalent but computationally more convenient representation of the potential [Eq. (15)], where the collective rotation is simply realized by changing each Euler angle ψ_χ. The appropriate permutations were then carried out. On the other hand, the choice in Eq. (14) appears to make comparisons with other potential models less cumbersome.

Before leaving this section, let us also notice that, in spite of the rather heavy computational cost, the investigated sample sizes are not very large (values $l \geq 40$ have been used in other simulation studies, e.g., Refs. [16,17]). Although a consistent qualitative picture seems to emerge (see results below), the quantitative accuracy of simulation results should be taken with caution or, better, left for further investigation in a future study, as happened with other similar cases in the literature.

VI. RESULTS AND COMPARISONS

We present here a selection of simulation results, and make appropriate comparison with the corresponding MF predictions. MF phase diagrams have been presented in Figs. 10 and 11, and transition temperatures are collected in Tables I and II, respectively.

Results for the mean potential energy U^* (mostly not shown) suggested a gradual and monotonic evolution with temperature, and their sample size dependency usually appeared to saturate between $l = 20$ and $l = 30$. The individual short-range order parameters (not shown) $\sigma_{L,j}$ were found to behave in a similar way.

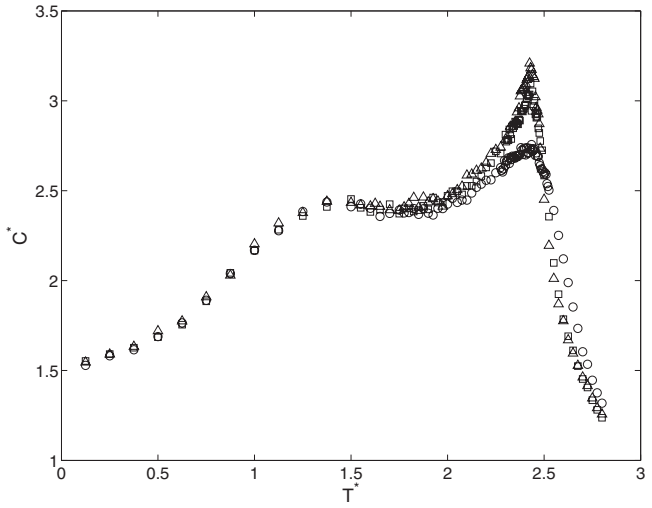

FIG. 12. Simulation results for the configurational specific heat of the μ model defined by $\mu = \frac{1}{4}$, obtained with different sample sizes. Same meaning of symbols as in Fig. 2. The plot exhibits a peak at $T^* \approx 2.4$, growing higher and sharper as sample size increases. On the other hand, simulation results for order parameters show a pronounced decrease with increasing sample size at and above this temperature (see Figs. 2–5); these two aspects are used to locate the transition temperature.

Simulation results for C^* were affected by statistical errors ranging between 1 and 5 %, not shown in the appropriate figures. For other reported observables, statistical errors fell within symbol sizes. In all investigated cases, the configurational specific heat C^* was found to be essentially independent of sample size, with the exception of a certain temperature range where it exhibited a peak, recognizably sharpening with increasing sample size. Simulation results for order parameters were also found to exhibit a pronounced decrease with increasing l, in and above the named temperature range. Thus the transition temperature Θ_{MC} was estimated on the largest sample, by combining the two named pieces of information; its uncertainty was conservatively taken to be twice the temperature step used in the transition region; comparison between MF and MC predictions for order parameters has been realized in various figures by plotting them versus T^*/Θ, i.e., scaling temperatures by the respective transition values.

Case $\mu = (1/4)$. The configurational specific heat C^* is shown in Fig. 12. Upon comparison with the corresponding results obtained for other values of μ, the height of the peak, as defined by the largest sample size, was found to decrease with increasing μ (see Fig. 13).

MF predicts in this case a direct isotropic-to-biaxial transition, and, in the ordered phase, relationships in Eqs. (47) hold. Simulation results confirm the direct transition and show that, in the ordered phase, the named relationships are better satisfied in the low-temperature régime. The overall agreement with MF results remained satisfactory even at high temperatures (Figs. 2–5).

Actually, for $\mu = (1/4), (1/2)$, both $\langle s_1 \rangle$ and $\langle s_4 \rangle$ were found to decrease monotonically with temperature (Figs. 2

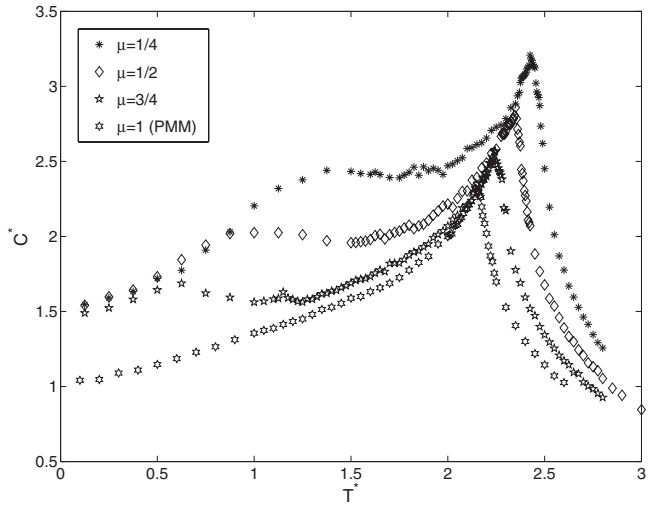

FIG. 13. Simulation results for specific heats of the μ models, obtained with the largest investigated sample size ($l=30$). Asterisks: $\mu=1/4$, diamonds: $\mu=1/2$, stars: $\mu=3/4$, hexagrams: $\mu=1$. The maxima fall between $T^*=2$ and $T^*=2.5$, and help locating transitions to the isotropic phases (see., e.g., Figs. 6–9).

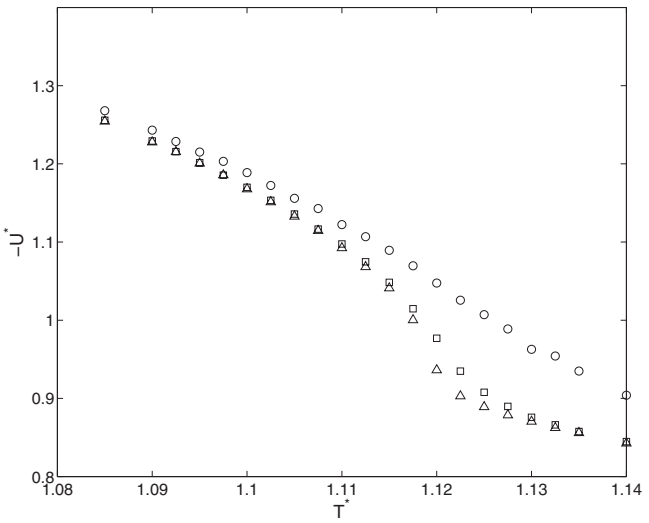

FIG. 14. Simulation results for the potential energy of the η model defined by $\eta=\frac{1}{4}$, in the transition region, and obtained with different sample sizes. Same meaning of symbols as in Fig. 2.

and 5). On the other hand, $\langle s_2\rangle$ and $\langle s_3\rangle$ showed a simple maximum taking place at $T^*/\Theta\approx 3/4$ (Figs. 3 and 4). Moreover, both MF and simulation results (figures not reported here) indicate that, at a given temperature in the ordered phase, the two order parameters $\langle s_1\rangle$ and $\langle s_4\rangle$ decrease upon increasing μ from 1/4 to 1/2.

Case $\mu=(1/2)$. Simulation results obtained for $\mu=(1/2)$ were found to be rather similar to their $\mu=(1/4)$ counterparts. Notice that, for $\mu=(1/4)$, MF predicts a direct transition between a low-temperature biaxial phase, where only two order parameters are independent [see Eqs. (47)], and the isotropic one. On the other hand, for $\mu=(1/2)$ MF predicts an intermediate uniaxial phase in the range $\Theta_{\mathrm{MF}}>T^*>T_A$, as well as a very narrow temperature range $T_B<T^*<T_A$, where the phase is biaxial and all four order parameters do not comply with Eqs. (47).

Case $\mu=(3/4)$. MF and simulation results for the order parameters obtained with $\mu=(3/4)$ exhibited another, more complex scenario: all the four order parameters showed a monotonic dependence on temperature for $T^*\lesssim 0.875$ and then $T^*\gtrsim 1.75$, but pronounced maxima and minima in between (points $\{\mathsf{M}_k,\mathsf{N}_k\}_{k=1,\ldots,4}$ in Figs. 6–9), together with a recognizable sample-size dependency. More precisely, upon increasing temperature from 0, $\langle s_1\rangle$, $\langle s_2\rangle$, $\langle s_3\rangle$ were found to evolve in a monotonic way up to a point N_k $(k=1,2,3)$, where their temperature profile changed from increasing to decreasing (or vice versa), and remained monotonic up to a point M_k. $\langle s_1\rangle$ became again monotonically decreasing at higher temperatures, whereas both $\langle s_2\rangle$ and $\langle s_3\rangle$ exhibited an additional maximum beyond M_2 and M_3, respectively. Notice also that, in Fig. 9, N_4 marks a change of slope, whereas M_4 is associated with a minimum. The pairs of points $(\mathsf{N}_k,\mathsf{M}_k)$ correspond to the pairs $(\mathsf{B}_k,\mathsf{A}_k)$ obtained by the above MF treatment, exhibiting abrupt changes of slopes associated with second-order transitions.

A simple interpretation can be put forward: as μ increases towards 1, biaxial order tends to be disturbed and reduced, and the uniaxial one to be favored (see the remark in the stability section). This effect is somehow strengthened and anticipated by MF, whereas MC suggests that even larger values of μ would be needed to fully stabilize a uniaxial phase, and point to the survival of a weakened biaxial phase up to the disordering transition. Notice also that MF predicts a constant value for the disordering transition temperature for $0\leq\mu\leq 1$, whereas simulation results show its linear decay with μ, and a slope ≈ -0.36.

Cases $\eta=(1/4),(1/2),(3/4)$. Results obtained for the three named values of the η parameter were qualitatively rather similar, so that only some results for $\eta=\frac{1}{4}$ will be discussed. The configurational specific heat C^* was again found to be independent of sample size with the exception of the transition range, where the height of its peak kept increasing with increasing sample size. Over the same temperature range, U^* exhibited a more explicit sample-size dependency (Figs. 14 and 15). The peak of the specific heat was again found to exhibit a recognizable decrease with increasing η (Fig. 16).

Simulation results for the order parameter $\langle s_1\rangle$ (Fig. 17) exhibited a monotonic decay with temperature, and again a more pronounced sample-size dependency in the transition range. Simulation results for $\langle s_3\rangle$ (Fig. 18) were found to increase with increasing temperature up to a peak near the transition temperature. Simulation results for $\langle s_2\rangle$ and $\langle s_4\rangle$ (not shown) remained smaller than 0.03, and kept decreasing with increasing sample size. $\langle s_2\rangle$ was found to peak around the transition, whereas $\langle s_4\rangle$ kept decreasing with increasing temperature. These results point to the vanishing of the named quantities in the thermodynamic limit. For $0<\eta<1$ MF predicts a first-order transition, whose transition temperature increases, and whose first-order character decreases with increasing η, thus becoming weaker and weaker in comparison with LL (for which an accurate characterization by simulation is a computationally demanding task [103–107]). The present simulation results are broadly compatible with a weak first-order transition, with transition

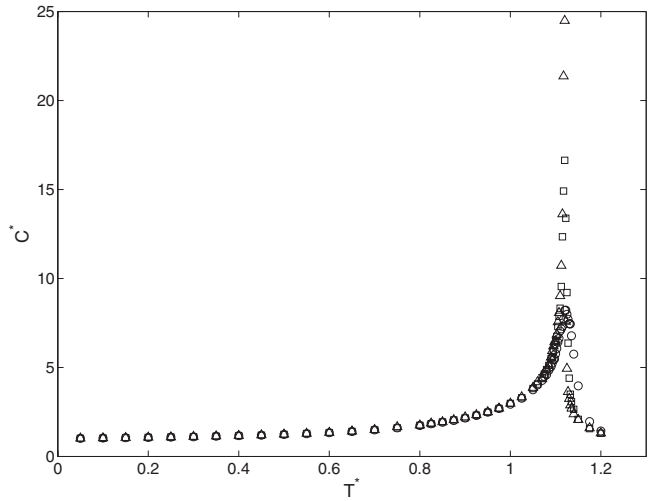

FIG. 15. Simulation results for the configurational specific heat of the η model defined by $\eta=\frac{1}{4}$, obtained with different sample sizes. Same meaning of discrete symbols as in Fig. 2.

jumps slowly developing with increasing sample size, but they do not completely exclude a second-order behavior.

On the other hand (see Fig. 11 and Table II), MF predicts a pronounced increase of the transition temperature upon increasing η from 0 to 1 (by some 30%), whereas simulation results point to its far weaker decrease (by $\approx$5%). In this case a least-square fit to a straight line was not satisfactory; a parabolic least-square fit was performed and the resulting curve was found to possess equation $\Theta_{\mathrm{MC,fit}}(\eta) = -0.02658\eta^2 - 0.02412\eta + 1.1232$.

Case $\eta=\mu=1$. The configurational specific heat C^* (Fig. 19) was again found to be independent of sample size with the exception of the transition range, where the height of its peak kept increasing with increasing sample size. Simulation results for the order parameter $\langle s_1\rangle$ (Fig. 20) exhibited a monotonic decay with temperature, and again a more pronounced sample-size dependency in the transition range.

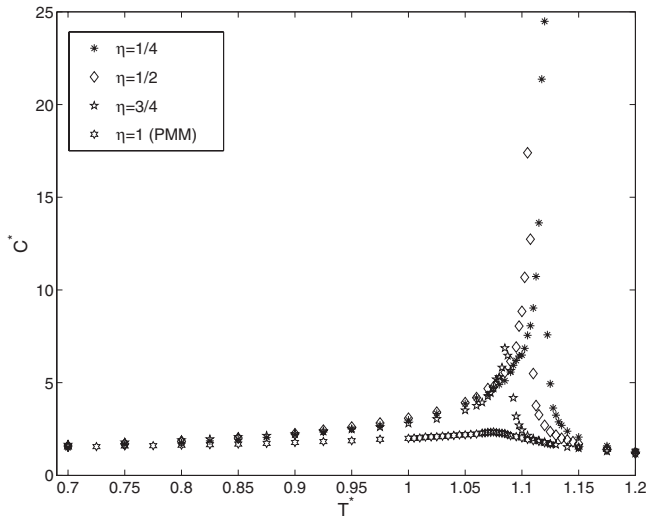

FIG. 16. Simulation results for specific heats of the η models, obtained with the largest investigated sample size ($l=30$). Asterisks: $\eta=1/4$, Diamonds: $\eta=1/2$, Stars: $\eta=3/4$, Hexagrams: $\eta=1$.

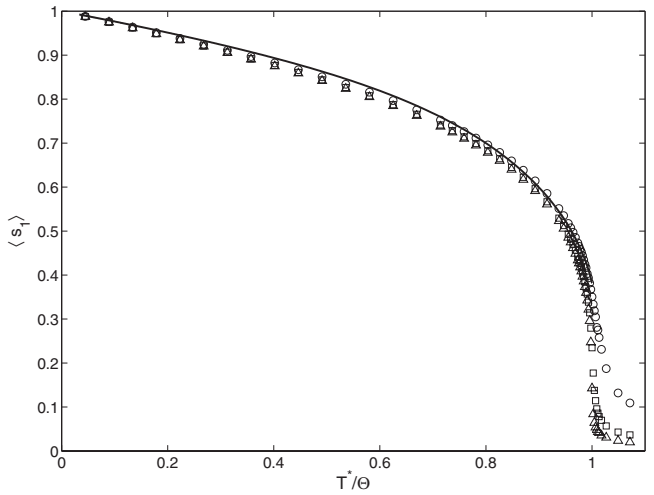

FIG. 17. MF predictions (continuous curve) and simulation results (discrete symbols) for the order parameter $\langle s_1\rangle$ of the η model defined by $\eta=\frac{1}{4}$, obtained with different sample sizes. Same meaning of symbols as in Fig. 2.

Simulation results for $\langle s_3\rangle$ (Fig. 21) were found to increase with increasing temperature up to a peak taking place at $T^*/\Theta \approx 0.8$, i.e., recognizably below the transition temperature. Simulation results for $\langle s_2\rangle$ and $\langle s_4\rangle$ (Figs. 22 and 23) remained smaller than 0.1, and exhibited a pronounced decrease with increasing sample size. They both peaked approximately at the same temperature as $\langle s_3\rangle$. These results again suggest to the vanishing of the named quantities in the thermodynamic limit.

Thus, on the whole, comparisons show a rough qualitative agreement between MF and simulation results. On the one hand, MF predictions involving the type of orientational order (whether uniaxial or biaxial) in the low-temperature phase do agree with simulation results. Predictions of direct second-order transitions between biaxial and isotropic phases (for the μ models, $0 \le \mu < 1$) also appear to be supported by

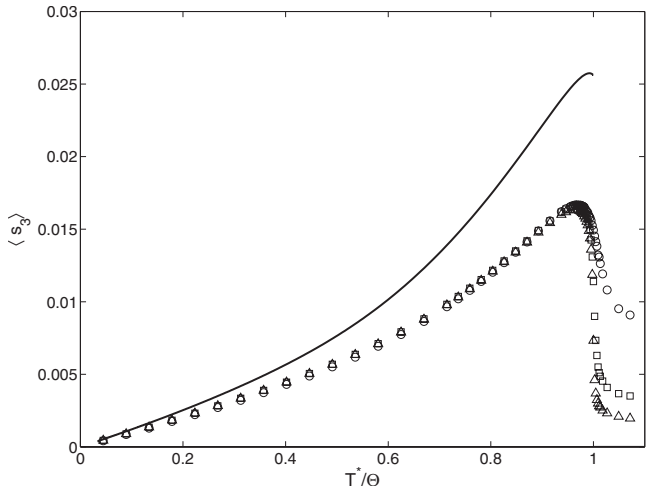

FIG. 18. MF predictions (continuous curve) and simulation results (discrete symbols) for the order parameter $\langle s_3\rangle$ of the η model defined by $\eta=\frac{1}{4}$, obtained with different sample sizes. Same meaning of symbols as in Fig. 2.

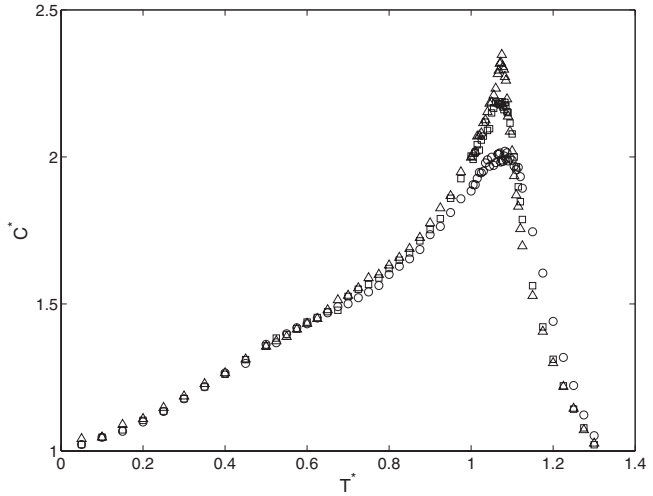

FIG. 19. Simulation results for the configurational specific heat of the PMM model, obtained with different sample sizes. Same meaning of symbols as in Fig. 2.

simulation, and similarly happens for the case $\eta=\mu=1$, where a second-order transition to a uniaxial phase is predicted. On the other hand, the MF prediction of an intermediate uniaxial phase for a certain range of μ values is not confirmed by the present simulations, even though the temperature profiles of order parameters are in good qualitative agreement (Figs. 6–9). Moreover, as pointed out above, Figs. 10 and 11 show that MF predictions concerning η or μ dependencies of transition temperatures disagree with simulation. It may be appropriate to recall that comparisons between MF predictions and MC results for the phase diagram of the above "dispersion" model on a three-dimensional lattice [16,17] showed a better qualitative agreement.

VII. CONCLUSIONS

To summarize, the investigated pair potentials depend on three parameters, whose ranges can be first significantly reduced by means of available geometric identities [77]. Some specific parameter ranges, discussed here, entail a stable biaxial pair (and hence overall) ground state, and the corresponding models (μ models) produce biaxial nematic behavior at low temperature. They can support a direct second-order transition between biaxial and isotropic phases, even though the interaction contains repulsive components. Both MF and MC treatments have shown that in case of strong repulsion the biaxial phase is weakened in the high-temperature regime and, according to MF, it can be even replaced by an intermediate uniaxial phase.

On the other hand, we have also considered parameter values producing uniaxial ground states (η models) in order, so to speak, to substantiate and to revisit the common remark about mesogenic molecules usually being biaxial but also usually producing uniaxial nematic phases. The corresponding pair potential models predict both first- and second-order

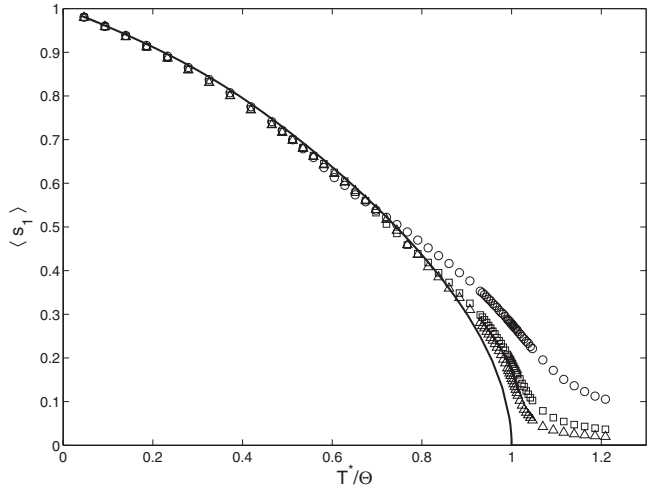

FIG. 20. MF predictions (continuous curve) and simulation results (discrete symbols) for the order parameter $\langle s_1 \rangle$ of the PMM model, obtained with different sample sizes. Same meaning of symbols as in Fig. 2.

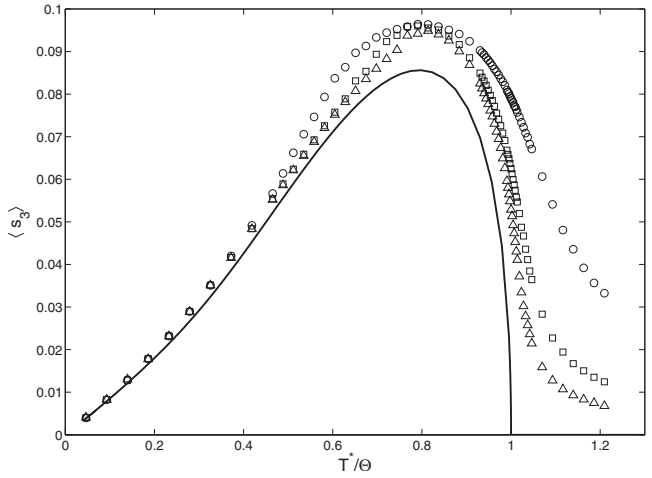

FIG. 21. MF predictions (continuous curve) and simulation results (discrete symbols) for the order parameter $\langle s_3 \rangle$ of the PMM model, obtained with different sample sizes. Same meaning of discrete symbols as in Fig. 2.

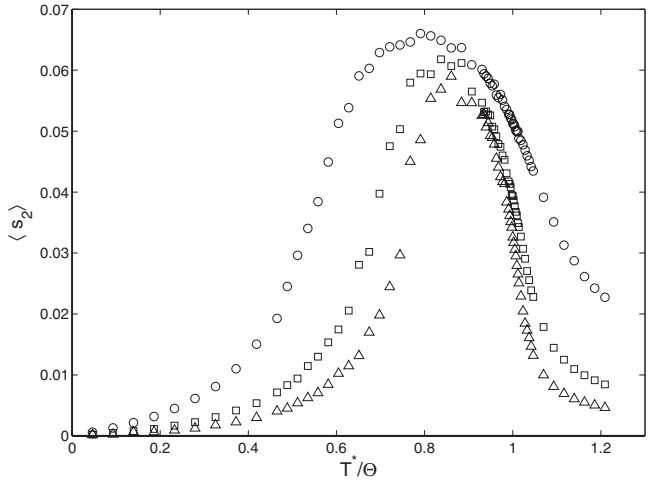

FIG. 22. Simulation results (discrete symbols) for the order parameter $\langle s_2 \rangle$ of the PMM model, obtained with different sample sizes. Same meaning of symbols as in Fig. 2. In this case the corresponding MF prediction is zero.

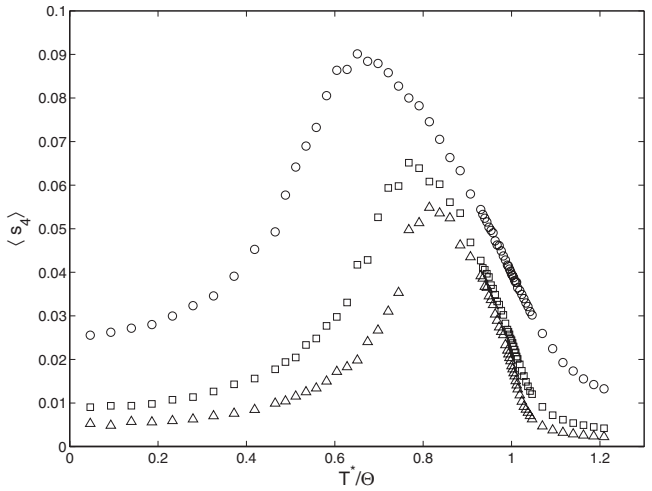

FIG. 23. Simulation results (discrete symbols) for the order parameter $\langle s_4 \rangle$ of the PMM model, obtained with different sample sizes. Same meaning of symbols as in Fig. 2. In this case the corresponding MF prediction is zero.

transitions between uniaxial and isotropic phases. In particular, the second-order transition occurs for the PMM case, which can be regarded as common limiting case for the two families of potential models.

Notice that, in experimental terms, the uniaxial nematic-isotropic transition is usually first order, but some rare example showing evidence of tricritical behavior in a nearly second-order case has been reported in Ref. [110] where a cyclic liquid crystalline trimer has been employed.

Since the investigated potential model has proven to be rather versatile, it also seems natural to consider other conditions under which biaxial behavior is completely removed from the resulting phase diagram. Actually, in the model parameter space, away from the named biaxial stability region, ground state configurations other than biaxial ones become allowed, and other potential models (even fully repulsive) deserve closer study, possibly giving rise to unexpected ordered phases. Investigations along these lines are currently under way, and will be reported in due course.

ACKNOWLEDGMENTS

The present extensive calculations were carried out on, among other machines, workstations belonging to the Sezione di Pavia of Istituto Nazionale di Fisica Nucleare (INFN). Allocations of computer time by the Computer Centre of Pavia University and CILEA (Consorzio Interuniversitario Lombardo per l' Elaborazione Automatica, Segrate–Milan) as well as by CINECA (Centro Interuniversitario Nord-Est di Calcolo Automatico, Casalecchio di Reno–Bologna), are gratefully acknowledged. The authors also wish to thank Professor L. Longa (Krakow, Poland), Professor G. R. Luckhurst (Southampton, England, UK), and Professor E. G. Virga (Pavia, Italy) for helpful discussion and suggestions.

[1] M. J. Freiser, Phys. Rev. Lett. **24**, 1041 (1970).
[2] M. J. Freiser, Mol. Cryst. Liq. Cryst. **14**, 165 (1971).
[3] R. Alben, Phys. Rev. Lett. **30**, 778 (1973).
[4] J. P. Straley, Phys. Rev. A **10**, 1881 (1974).
[5] G. R. Luckhurst, C. Zannoni, P. L. Nordio, and U. Segre, Mol. Phys. **30**, 1345 (1975).
[6] N. Boccara, R. Mejdani, and L. De Seze, J. Phys. (Paris) **38**, 149 (1976).
[7] D. K. Remler and A. D. J. Haymet, J. Phys. Chem. **90**, 5426 (1986).
[8] B. Bergersen, P. Palffy-Muhoray, and D. A. Dunmur, Liq. Cryst. **3**, 347 (1988).
[9] Zhang Zhi-Dong and Huang Xi-Min, Acta Phys. Sin. (Overseas Ed.) **6**, 671 (1997).
[10] M. Hosino and H. Nakano, Mol. Cryst. Liq. Cryst. Sci. Technol., Sect. A **348**, 207 (2000).
[11] D. W. Allender and M. A. Lee, Mol. Cryst. Liq. Cryst. **110**, 331 (1984).
[12] D. W. Allender, M. A. Lee, and N. Hafiz, Mol. Cryst. Liq. Cryst. **124**, 45 (1985).
[13] E. F. Gramsbergen, L. Longa, and W. H. de Jeu, Phys. Rep. **135**, 195 (1986).
[14] G. R. Luckhurst and S. Romano, Mol. Phys. **40**, 129 (1980).
[15] C. D. Mukherjee and N. Chatterjee, Phys. Lett. A **189**, 86 (1994).
[16] F. Biscarini, C. Chiccoli, P. Pasini, F. Semeria, and C. Zannoni, Phys. Rev. Lett. **75**, 1803 (1995).
[17] C. Chiccoli, P. Pasini, F. Semeria, and C. Zannoni, Int. J. Mod. Phys. C **10**, 469 (1999).
[18] P. Pasini, C. Chiccoli, and C. Zannoni, *Advances in the Computer Simulations of Liquid Crystals*, edited by P. Pasini and C. Zannoni, Vol. 545 of *NATO Science Series C* (Kluwer, Dordrecht, 2000), Chap. 5.
[19] C. Shih and R. Alben, J. Chem. Phys. **57**, 3057 (1972).
[20] B. M. Mulder, Liq. Cryst. **1**, 539 (1986).
[21] B. Mulder, Phys. Rev. A **39**, 360 (1989).
[22] R. Hołyst and A. Poniewierski, Mol. Phys. **69**, 193 (1990).
[23] B. M. Mulder, Liq. Cryst. **8**, 527 (1990).
[24] M. P. Taylor and J. Herzfeld, Phys. Rev. A **44**, 3742 (1991).
[25] B. Tjipto-Margo and G. T. Evans, J. Chem. Phys. **94**, 4546 (1991).
[26] A. N. Zakhlevnykh and P. A. Sosnin, Mol. Cryst. Liq. Cryst. Sci. Technol., Sect. A **293**, 135 (1997).
[27] P. I. C. Teixeira, A. J. Masters, and B. M. Mulder, Mol. Cryst. Liq. Cryst. Sci. Technol., Sect. A **323**, 167 (1998).
[28] M. P. Allen, Liq. Cryst. **8**, 499 (1990).
[29] P. J. Camp and M. P. Allen, J. Chem. Phys. **106**, 6681 (1997).
[30] P. J. Camp, M. P. Allen, and A. J. Masters, J. Chem. Phys. **111**, 9871 (1999).
[31] M. A. Bates and G. R. Luckhurst, Struct. Bonding (Berlin) **94**, 65 (1998).
[32] R. Berardi, C. Fava, and C. Zannoni, Chem. Phys. Lett. **236**, 462 (1995).
[33] G. Ayton and G. N. Patey, J. Chem. Phys. **102**, 9040 (1995).

[34] D. J. Cleaver, C. M. Care, M. P. Allen, and M. P. Neal, Phys. Rev. E **54**, 559 (1996).
[35] S. Sarman, J. Chem. Phys. **104**, 342 (1996).
[36] V. V. Ginzburg, M. A. Glaser, and N. A. Clark, Chem. Phys. **214**, 253 (1997).
[37] R. Berardi and C. Zannoni, J. Chem. Phys. **113**, 5971 (2000).
[38] R. Berardi, L. Muccioli, and C. Zannoni, J. Chem. Phys. **128**, 024905 (2008).
[39] B. Mettout, P. Tolédano, H. Takezoe, and J. Watanabe, Phys. Rev. E **66**, 031701 (2002).
[40] B. Mettout, Phys. Rev. E **72**, 031706 (2005).
[41] B. Mettout, Phys. Rev. E **74**, 041701 (2006).
[42] S. Romano, Physica A **339**, 511 (2004).
[43] G. R. Luckhurst, J. Jpn. Soc. Technol. Plast. **44**, 2834 (2005).
[44] M. A. Bates and G. R. Luckhurst, Phys. Rev. E **72**, 051702 (2005).
[45] M. A. Bates, Chem. Phys. Lett. **437**, 189 (2007).
[46] A. Ferrarini, P. L. Nordio, E. Spolaore, and G. R. Luckhurst, J. Chem. Soc., Faraday Trans. **91**, 3177 (1995).
[47] M. A. Bates and G. R. Luckhurst, Phys. Chem. Chem. Phys. **7**, 2821 (2005).
[48] M. A. Bates, Phys. Rev. E **74**, 061702 (2006).
[49] L. J. Yu and A. Saupe, Phys. Rev. Lett. **45**, 1000 (1980).
[50] J. Malthête, L. Liebert, A.-M. Levelut, and Y. Galerene, C. R. Acad. Sci., Ser. II: Mec., Phys., Chim., Sci. Terre Univers **303**, 1073 (1986).
[51] K. Praefcke, B. Kohne, B. Gündoğan, D. Singer, D. Demus, S. Diele, G. Pelzl, and U. Bakowsky, Mol. Cryst. Liq. Cryst. **198**, 393 (1991).
[52] S. Chandrasekhar, Mol. Cryst. Liq. Cryst. Sci. Technol., Sect. A **243**, 1 (1994).
[53] S. Chandrasekhar, G. G. Nair, D. S. Shankar Rao, S. Krishna Prasad, K. Praefcke, and D. Blunk, Curr. Sci. **75**, 1042 (1998).
[54] S. M. Fan, I. D. Fletcher, B. Gündoğan, N. J. Heaton, G. Kothe, G. R. Luckhurst, and K. Praefcke, Chem. Phys. Lett. **204**, 517 (1993).
[55] G. R. Luckhurst, Thin Solid Films **393**, 40 (2001).
[56] K. Praefcke, Mol. Cryst. Liq. Cryst. Sci. Technol., Sect. A **364**, 15 (2001).
[57] K. Praefcke, Braz. J. Phys. **32**, 564 (2002).
[58] B. R. Acharya, A. Primak, and S. Kumar, Liq. Cryst. Today **13**, 1 (2004).
[59] L. A. Madsen, T. J. Dingemans, M. Nakata, and E. T. Samulski, Phys. Rev. Lett. **92**, 145505 (2004).
[60] B. R. Acharya, A. Primak, and S. Kumar, Phys. Rev. Lett. **92**, 145506 (2004).
[61] G. R. Luckhurst, Nature (London) **430**, 413 (2004).
[62] J.-H. Lee, T.-K. Lim, W.-T. Kim, and J.-I. Jin, J. Appl. Phys. **101**, 034105 (2007).
[63] Y. Galerne, Phys. Rev. Lett. **96**, 219803 (2006).
[64] L. A. Madsen, T. J. Dingemans, M. Nakata, and E. T. Samulski, Phys. Rev. Lett. **96**, 219804 (2006).
[65] K. Merkel, A. Kocot, J. K. Vij, R. Korlacki, G. H. Mehl, and T. Meyer, Phys. Rev. Lett. **93**, 237801 (2004).
[66] J. L. Figueirinhas, C. Cruz, D. Filip, G. Feio, A. C. Ribeiro, Y. Frère, T. Meyer, and G. H. Mehl, Phys. Rev. Lett. **94**, 107802 (2005).
[67] K. Neupane, S. W. Kang, S. Sharma, D. Carney, T. Meyer, G. H. Mehl, D. W. Allender, S. Kumar, and S. Sprunt, Phys. Rev. Lett. **97**, 207802 (2006).
[68] K. Severing and K. Saalwächter, Phys. Rev. Lett. **92**, 125501 (2004).
[69] K. Severing, E. Stibal-Fischer, A. Hasenhindl, H. Finkelmann, and K. Saalwächter, J. Phys. Chem. B **110**, 15680 (2006).
[70] J. You, J. Y. Jung and K. Rhie, V. M. Pergamenshchik, S. T. Shin, J. Korean Phys. Soc. **52**, 342 (2008).
[71] V. Cîrcus, P. N. Horton, M. B. Hursthouse, and D. W. Bruce, Liq. Cryst. **34**, 1463 (2007).
[72] A. M. Sonnet, E. G. Virga, and G. E. Durand, Phys. Rev. E **67**, 061701 (2003).
[73] G. De Matteis and E. G. Virga, Phys. Rev. E **71**, 061703 (2005).
[74] F. Bisi, E. G. Virga, E. C. Gartland, Jr., G. De Matteis, A. M. Sonnet, and G. E. Durand, Phys. Rev. E **73**, 051709 (2006).
[75] D. Pociecha, E. Gorecka, M. Cepic, N. Vaupotic, and W. Weissflag, Phys. Rev. E **74**, 021702 (2006).
[76] G. De Matteis, F. Bisi and E. G. Virga, Continuum Mech. Thermodyn. **19**, 1 (2007).
[77] S. Romano, Physica A **337**, 505 (2004).
[78] S. Romano, Phys. Lett. A **333**, 110 (2004).
[79] G. De Matteis, S. Romano, and E. G. Virga, Phys. Rev. E **72**, 041706 (2005).
[80] Z.-D. Zhang, Y.-J. Zhang, and Z.-L. Sun, Chin. Phys. Lett. **23**, 3025 (2006).
[81] D. Allender and L. Longa, e-print arXiv:0712.3055v1.
[82] G. De Matteis, A. M. Sonnet, and E. G. Virga (unpublished).
[83] G. Lasher, Phys. Rev. A **5**, 1350 (1972).
[84] P. I. C. Teixeira, M. A. Osipov, and G. R. Luckhurst, Phys. Rev. E **73**, 061708 (2006).
[85] J. Peláez and M. R. Wilson, Phys. Rev. Lett. **97**, 267801 (2006).
[86] D. M. Brink and G. R. Satchler, *Angular Momentum*, 2nd ed. (Oxford University Press, Oxford, UK, 1968).
[87] D. A. Varshalovich, A. N. Moskalev, and V. K. Khersonskii, *Quantum Theory of Angular Momentum* (World Scientific, Singapore, 1988).
[88] G. B. Arfken and H. J. Weber, *Mathematical Methods for Physicists*, 4th ed. (Academic Press, San Diego, 1995).
[89] L. Longa, P. Grzybowski, S. Romano, and E. Virga, Phys. Rev. E **71**, 051714 (2005); **73**, 019904 (2006).
[90] L. Longa and G. Pajak, Liq. Cryst. **32**, 1409 (2005).
[91] A. D. Buckingham, in *Intermolecular Forces*, Vol. 12 of Adv. Chem. Phys., edited by J. O. Hirschfelder (Interscience, New York, 1967), Chap. 2, pp. 107–142.
[92] C. G. Gray and K. E. Gubbins, *Theory of Molecular Fluids* (Oxford University Press, Oxford, UK, 1984), Vol. 1.
[93] S. Romano, Physica A **339**, 491 (2004).
[94] R. F. Kayser, Jr., H. J. Raveché, Phys. Rev. A **17**, 2067 (1978).
[95] C. Zannoni, *The Molecular Physics of Liquid Crystals*, edited by G. R. Luckhurst and G. W. Gray (Academic Press, London, 1979), Chaps. 3 and 9.
[96] C. Zannoni, *Advances in the Computer Simulations of Liquid Crystals*, edited by P. Pasini and C. Zannoni, Vol. 545 of NATO Science Series, (Kluwer, Dordrecht, 2000) Chap. 2.
[97] G. R. Luckhurst, *Physical Properties of Liquid Crystals: Nematics*, edited by D. A. Dunmur, A. Fukuda and G. R. Luckhurst (INSPEC, London, UK, 2001), Chap. 2.1.
[98] N. N. Bogolubov, Jr., *A Method for Studying Model Hamiltonians: A Minimax Principle for Problems in Statistical Physics* (Pergamon Press, Oxford, 1972).

[99] N. N. Bogolubov, Jr., B. I. Sadovnikov, and A. S. Shumosky, *Mathematical Methods of Statistical Mechanics of Model Systems* (CRC Press, Boca Raton, FL, 1994).
[100] M. A. Osipov and A. S. Shumovskii, Teor. Mat. Fiz. **46**, 125 (1981) [Theor. Math. Phys. **46**, 83 (1981)].
[101] Willy J. F. Govaerts, *Numerical Methods for Bifurcations of Dynamical Equilibria* (SIAM, Philadelphia, 2000).
[102] E. J. Doedel, R. C. Paffenroth, A. R. Champneys, T. F. Fairgrieve, Y. A. Kuznetsov, B. E. Oldeman, B. Sandstede, and X. Wang (unpublished).
[103] U. Fabbri and C. Zannoni, Mol. Phys. **58**, 763 (1986).
[104] Z. Zhang, O. G. Mouritsen, and M. J. Zuckermann, Phys. Rev. Lett. **69**, 2803 (1992).
[105] Z. Zhang, M. J. Zuckermann, and O. G. Mouritsen, Mol. Phys. **80**, 1195 (1993).
[106] C. W. Greeff and M. A. Lee, Phys. Rev. E **49**, 3225 (1994).
[107] D. Gonin and A. H. Windle, Liq. Cryst. **23**, 489 (1997).
[108] T. Matsui, T. Hofsass, and H. Kleinert,Phys. Rev. A **33**, 660 (1986).
[109] R. Hashim and S. Romano, Int. J. Mod. Phys. B **13**, 3879 (1999).
[110] I. M. Syed, V. Percec, R. G. Petschek, and C. Rosenblatt, Phys. Rev. E **67**, 011704 (2003).